Archive of Applied Mechanics manuscript No.
(will be inserted by the editor)

Paul Steinmann · Mokarram Hossain · Gunnar Possart

Hyperelastic models for rubber-like materials: Consistent tangent operators and suitability for Treloar's data

Received: date / Accepted: date

Abstract Rubber-like materials consist of chain-like macromolecules that are more or less closely connected to each other via entanglements or cross-links. As an idealisation, this particular structure can be described as a completely random three-dimensional network. To capture the elastic and nearly incompressible mechanical behaviour of this material class, numerous phenomenological and micro-mechanically motivated models have been proposed in the literature.

This contribution reviews fourteen selected representatives of these models whereas the main focus lies on the derivation of accurate and thermodynamically consistent tangent operators. The latter, although prevalently missing in the literature, are indispensable ingredients in utilising any kind of constitutive model for the numerical solution of boundary value problems by iterative approaches like the Newton-Raphson scheme. Furthermore, the performances provided by the models in reproducing the classical experimental data of Treloar [1] are evaluated.

Keywords rubber-like material · hyperelasticity · phenomenological model · micro-mechanical model

1 Introduction and Outline

Since the beginning of the 20th century, the mechanics of rubber-like materials has been a very active field of research due to their wide range of applications. In particular, the demand for predictive analysis tools facilitating the economic design of complex devices for different loading conditions is continuosly increasing. Famous rubber applications are e.g. tires, seals, conveyor belts, base isolations of buildings and many more [2],[3]. In the last few decades, developments in computational mechanics, especially in finite element methods, have enabled three-dimensional, large strain analyses of complex elastomeric products to be an integral part of design processes. This progress, vice versa, has led to a more critical assessment and further development of constitutive models for rubber elasticity since an accurate reproduction of the three-dimensional stress-strain behaviour is indispensable for any numerical simulation of complex deformations [4].

The starting point of hyperelastic material modelling is the formulation of a scalar *strain (or stored or potential) energy function*. Such functions usually depend either on strain tensors like the right (or left) Cauchy-Green tensor $\boldsymbol{C} = \boldsymbol{F}^t\boldsymbol{F}$ (or $\boldsymbol{b} = \boldsymbol{F}\boldsymbol{F}^t$) with $\boldsymbol{F} = \partial\boldsymbol{\varphi}/\partial\boldsymbol{X}$ being the material gradient of the nonlinear deformation map $\boldsymbol{\varphi}$, on invariants of these strain tensors, i.e. $I_1(\boldsymbol{C}) = \mathrm{tr}(\boldsymbol{C}) = I_1(\boldsymbol{b})$, $I_2(\boldsymbol{C}) = \frac{1}{2}[\mathrm{tr}^2(\boldsymbol{C}) - \mathrm{tr}(\boldsymbol{C}^2)] = I_2(\boldsymbol{b})$, $I_3(\boldsymbol{C}) = \det(\boldsymbol{C}) = I_3(\boldsymbol{b})$, or directly on the principal stretches $\lambda_1, \lambda_2, \lambda_3$, which are the square roots of the eigenvalues of $\boldsymbol{C}$.

Every model for rubber-like materials can, in general, be classified as **phenomenological** or **micro-mechanical**. The latter are derived from statistical mechanics arguments on networks of idealised chain

Paul Steinmann, Mokarram Hossain, Gunnar Possart
Chair of Applied Mechanics, University of Erlangen-Nuremberg, Germany
Tel:+49-9131-8528501
Fax: +49-9131-8528503
E-mail: steinmann@ltm.uni-erlangen.de,hossain@ltm.uni-erlangen.de,possart@ltm.uni-erlangen.de

molecules, cf. e.g. [5], whereas the former utilise more or less complex, frequently polynomial formulations in terms of strain invariants or principal stretches. Although intrinsically tied to higher computational costs (and homogenisation requirements), micro-mechanical approaches recently got more and more attention due to the fact that their governing parameters – at least somehow – relate macroscopic mechanical behaviour to the causative physical/chemical structure [2]. This property is a significant advantage compared to phenomenological models, especially if e.g. gradients in the structural composition as observed at phase boundaries (interphases) or temporal changes in the network structure (curing) do occur and have to be described. Prominent examples for micro-mechanical models are the 3-chain, 4-chain, 8-chain models as well as the micro-macro unit sphere (21-chain) model which have all been proven to be very appropriate for moderate to large elastic deformations of rubber-like materials, cf. Arruda and Boyce [4],[6] and Miehe & co-workers [2],[7],[8],[9].

Among the numerous phenomenological approaches, the class of the celebrated Ogden models [10] represents a very flexible ansatz in modelling rubber-like materials, in particular due to its modular polynomial formulation in terms of principal stretches – which additionally makes it amenable to mathematical analysis. Also well-known, widely used and of earlier origin are models of Mooney-Rivlin type, cf. e.g. [11] or [12],[13],[14], which are formulated in strain invariants. Its simplest realisation, called neo-Hookean model, constitutes a close link to micro-mechanical approaches since it coincides with a 3-chain model using Gaussian chain statistics. The main challenge in designing invariant based models is to choose an appropriate (sub)set of invariants and to include sufficiently high orders of them into the strain energy function. As pointed out e.g. by Yeoh [15], already cubic terms of I_1 are able to reproduce the highly nonlinear, S-shaped uniaxial behaviour of rubber, also at very large strains. Nonetheless, using only reduced sets of invariants will always significantly impaire the model's behaviour at more complex, multiaxial deformation modes.

Also hybrid models merging phenomenological and micro-mechanical approaches to benefit from the advantages of both worlds have been proposed by different authors. Examples are Yeoh and Fleming [16] or Wu and van der Giessen [17] who combine 3-chain and 8-chain models by a phenomenological adjustment parameter. A different hybrid approach has been presented by Beda and Chevalier [19] who linked the Gent and Thomas model [20] with that of Ogden [10] to have appropriate ansatzes for both the small and large strain range. Additionally, a method to determine the material parameters has been proposed.

To assess the quality and accuracy that a particular model can achieve in reproducing real material behaviour, it is common practice to simulate homogeneous deformations and compare the results with experimental data. Since experiments are time consuming and cost intensive it is desirable to minimise their number and the complexity that is necessary to correctly determine the governing material parameters. Thus, the competing requirements read as follows: an ideal material model should **(1)** contain as few parameters as possible, **(2)** be able to correctly reproduce arbitrarily complex deformation behaviour, and, **(3)** allow the determination of its parameters for a specific material from fitting few simple experiments. Unfortunately, these properties are often reconcilable in real world applications and necessitate many compromises, as is documented by the vast number of publications dealing with different aspects of this matter. Any bibliography on this field essentially has to remain incomplete.

Concerning comparative studies, Marckmann and Verron [20], for example, analysed twenty different models and ranked them with respect to the classical Treloar data [1] indicating that the extended tube model [21], the Shariff model [22], the 21-chain model [2] and the Ogden model [10] provide the best results. The same approach was followed by Boyce and Arruda [4] who also compared five models using Treloar's experimental data for uniaxial, biaxial and pure shear deformations. Seibert and Schöche [23] compared six different models with respect to uniaxial and biaxial experimental data of a carbon-black filled rubber and conclude that higher order terms are essential to reproduce the typical increase in stiffness at large strains, even if such terms are susceptible to instability problems. Furthermore, it is stated that the Arruda-Boyce model provides reliable predictions of biaxial deformations although calibrated only with uniaxial data.

A higher order elasticity model, composed of a neo-Hookean-like compressible and a generalised Mooney-type incompressible component, has been proposed by Attard and Hunt [24] and was proven to perform excellent on experimental data of uniaxial and (equi)biaxial tension and pure shear from seven different authors. In particular, it is pointed out that this formulation is capable to reproduce the Valanis-Landel hypothesis [25] (experimentally approved by Vangerko and Treloar [26]), which states that interactions of principal stresses are governed only by compressive deformation parts whereas the incompressible strain energy density is represented by a superposition of terms dependent on the principal stretches. Chagnon et al. [27] compared the models of Hart-Smith [28], Arruda-Boyce [6] and Gent [29] stating similar responses and, furthermore, establishing equations to relate the material parameters. The similarity in behaviour of Arruda-Boyce and Gent model was also demonstrated by Boyce [30]. Another conceptual link between micro-mechanical and

phenomenological models has been discussed by Horgan and Saccomandi [31],[32] who showed that the two-parameter Gent model is an accurate approximation of a non-Gaussian full network model involving the inverse Langevin function. Furthermore, its phenomenological parameters can be formulated in terms of microscopic properties. A conceptually different and interesting approach to compare constitutive models for elastomers was proposed by Currie [33]. It uses the so-called attainable region in the invariant space of the free energy, which is a three-dimensional surface computable from different homogeneous deformation experiments by methods introduced in Haines and Wilson [34], to numerically compare different free energies. The advantage is that not only particular formulations or single deformation modes can be compared but the whole image spaces of specific models.

In order to apply arbitrary constitutive models within a nonlinear finite element framework it is essential not only to derive the corresponding stress-strain relation but also to determine an accurate and thermodynamically consistent tangent operator providing quadratic convergence while solving the governing nonlinear equations by iterative schemes like Newton-Raphson. The theoretical background to derive stress tensors and tangent operators from arbitrary strain energy functions for finite elasticity was, for example, given by Miehe [35], where main emphasis is put on different mixed finite element formulations necessary to capture incompressibility. Frameworks for the derivation of stress tensors and tangent operators for models based on invariants have been presented by Liu et al. [36] and Kaliske and Rothert [37], where the former contains details for both reference and current configurations while the latter is restricted to the current configuration.

In most publications on rubber elasticity, authors propose new constitutive models and analyse their performance by comparison with different, usually homogeneous experimental data like those from Treloar [1]. Unfortunately, only a minority of works provides both stress tensors and tangent operators for particular models, like e.g. Miehe and co-workers [2],[7],[9] did for the 21-chain model or Heinrich and Kaliske [38],[21] who introduced the extended tube model and provided details on the finite element implementation as well as a model verification by (non-)homogeneous numerical examples. To close this gap, the present contribution elaborately derives the tangent operators for a selection of both phenomenological and micro-mechanical models, which is complemented by a comparative study of the model performances with respect to the classical Treloar data.

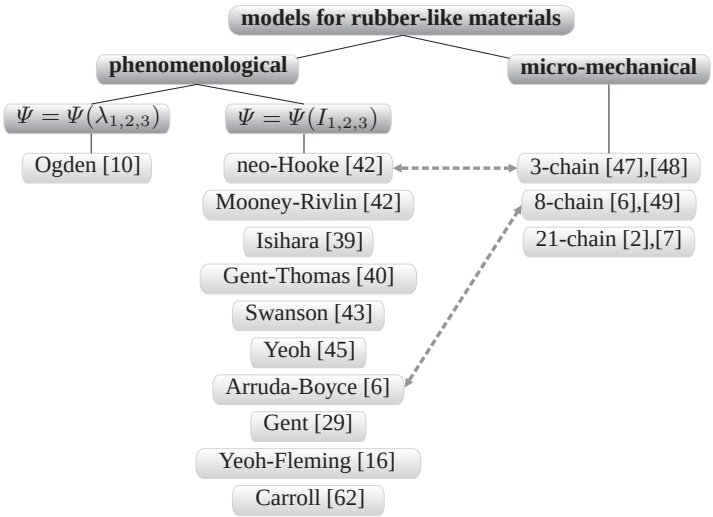

Fig. 1 The here considered hyperelastic models for rubber-like materials and some corresponding references

The **outline** of this paper is as follows: in Section 2 we briefly review the general framework for stress tensors and tangent operators for finite isotropic elasticity as developed in Miehe [35] and summarise the details for the special case of invariant based models as given by Liu et al. [36]. After these preliminaries, Sections 3 and 4 present a selection of fourteen constitutive models for elastic rubber-like materials, derive the corresponding equations for stress tensor and tangent operator from the strain energy function and demonstrate the quadratic convergence when iteratively solving boundary value problems. The models considered cover examples from both phenomenological (eleven) and micro-mechanical approaches (three) and are listed in Figure 1. Furthermore, Sections 3 and 4 each contain details on the derivation of analytical stress-strain relations from arbitrary free energy functions for the homogeneous cases of uniaxial tension, equibaxial ten-

sion and pure shear. These analytical formulations are then used to evaluate the performance of each model in reproducing the experimental data provided by Treloar, cf. Appendix A. To this end a standard fitting tool is applied to calculate optimal model parameters wrt each set of Treloar's data. Aiming at the above mentioned model requirement **(3)**, i.e. the ability of a model to be correctly adjusted for all deformation modes by as few as possible experiments, we further compare the errors that arise if each model together with the optimal parameters for a particular deformation mode is used to simulate the remaining two deformation modes. From this a surely not objective ranking of the models concludes this contribution.

2 Continuum mechanical preliminaries

The subsequent considerations are restricted to the case of isothermal isotropic hyperelastic material behaviour in the finite strain regime. We review the steps to derive stress tensors and tangent operators from a given strain energy density, for both formulations in terms of tensor-valued strain measures (cf. [35]) and for invariant based functions (cf. [36]).

2.1 Stress tensor and tangent operator derivation

The isothermal response of a hyperelastic material can be described by a strain energy function $\Psi = \Psi(\boldsymbol{C})$, which we assume to be dependent on the right Cauchy-Green tensor, i.e. all subsequent considerations take place in the material configuration. For a derivation of stresses and tangent operators in the spatial configuration we refer to e.g. [9],[42] or [37] for the case of invariant based free energy functions.

The second Piola-Kirchhoff stress tensor $\boldsymbol{S}$ is then given as twice the derivative of the free energy wrt $\boldsymbol{C}$ and by introducing the fourth-order elasticity tensor (or tangent operator) $\mathbb{C}$ one can describe changes in stress $\Delta\boldsymbol{S}$ that are caused by changes in deformation $\Delta\boldsymbol{C}$ via $\Delta\boldsymbol{S} = \mathbb{C} : \frac{1}{2}\Delta\boldsymbol{C}$, i.e.

$$\boldsymbol{S} = 2\frac{\partial\Psi}{\partial\boldsymbol{C}} \qquad , \qquad \mathbb{C} = 2\frac{\partial\boldsymbol{S}}{\partial\boldsymbol{C}} = 4\frac{\partial^2\Psi}{\partial\boldsymbol{C}^2}. \tag{1}$$

Since rubber-like materials usually exhibit a decoupled response to volumetric and deviatoric deformations an additive split of the strain energy function into volumetric (shape preserving) and isochoric (volume preserving but shape changing) parts can be motivated [7],[20],[37]:

$$\Psi(\boldsymbol{C}) = \Psi_{\mathrm{vol}}(J) + \Psi_{\mathrm{iso}}\big(\bar{\boldsymbol{C}}\big), \tag{2}$$

where $J = \det\boldsymbol{F}$ and $\bar{\boldsymbol{C}} = J^{-2/3}\boldsymbol{C}$ denotes the isochoric right Cauchy-Green tensor. Additive split (2) coincides with the multiplicative split $\boldsymbol{F} = [J^{1/3}\boldsymbol{I}]\bar{\boldsymbol{F}}$ of the deformation gradient that goes back to Flory [50] and satisfies the incompressibility condition $\det\bar{\boldsymbol{F}} = 1$. A combination of (1) and (2) yields the correspondingly decoupled stress tensor and tangent operator:

$$\boldsymbol{S} = \boldsymbol{S}_{\mathrm{vol}} + \boldsymbol{S}_{\mathrm{iso}} = 2\frac{\partial\Psi_{\mathrm{vol}}}{\partial\boldsymbol{C}} + 2\frac{\partial\Psi_{\mathrm{iso}}}{\partial\boldsymbol{C}} \qquad , \qquad \mathbb{C} = \mathbb{C}_{\mathrm{vol}} + \mathbb{C}_{\mathrm{iso}} = 2\frac{\partial\boldsymbol{S}_{\mathrm{vol}}}{\partial\boldsymbol{C}} + 2\frac{\partial\boldsymbol{S}_{\mathrm{iso}}}{\partial\boldsymbol{C}}. \tag{3}$$

From the chain rule and some algebraic manipulations the volumetric stress tensor can be reformulated as

$$\boldsymbol{S}_{\mathrm{vol}} = 2\frac{\partial\Psi_{\mathrm{vol}}(J)}{\partial J}\frac{\partial J}{\partial\boldsymbol{C}} = Jp\,\boldsymbol{C}^{-1}, \tag{4}$$

where the hydrostatic pressure $p = \partial\Psi_{\mathrm{vol}}(J)/\partial J$ has been introduced. In case of incompressibility, $J = 1$ and p serves as a Lagrange multiplier to satisfy this kinematic constraint on the deformation. The pressure can then only be calculated from the equilibrium equations together with boundary conditions. For compressible materials one usually prescribes some volumetric strain energy function in terms of a bulk modulus k_0 and a parameter β like e.g. $\Psi_{\mathrm{vol}}(J) = k_0\beta^{-2}[J^{-\beta} + \beta\ln(J) - 1]$ as given in [10].

To directly utilise formulations of Ψ_{iso} in terms of the isochoric right Cauchy-Green tensor $\bar{\boldsymbol{C}}$, the fictitious stress tensor $\bar{\boldsymbol{S}} = 2\partial\Psi_{\mathrm{iso}}(\bar{\boldsymbol{C}})/\partial\bar{\boldsymbol{C}}$ is introduced and the isochoric deviatoric stress $\boldsymbol{S}_{\mathrm{iso}}$ is then obtained via the fourth-order projection tensor $\mathbb{P} = \partial\bar{\boldsymbol{C}}/\partial\boldsymbol{C}$ by

$$\boldsymbol{S}_{\mathrm{iso}} = J^{-\frac{2}{3}}\mathbb{P} : \bar{\boldsymbol{S}} \qquad \text{with} \qquad \mathbb{P} = \mathbb{I} - \frac{1}{3}\boldsymbol{C}^{-1}\otimes\boldsymbol{C} \quad , \quad \mathbb{I} = \delta_{ik}\delta_{jl}. \tag{5}$$

From further evaluation of $(3)_2$, the details of which can be found e.g. in [42], one finally obtains the two parts of the tangent operator:

$$\mathbb{C}_{\text{vol}} = \left[Jp + J^2 \frac{dp}{dJ} \right] \boldsymbol{C}^{-1} \otimes \boldsymbol{C}^{-1} - 2Jp\, \boldsymbol{C}^{-1} \odot \boldsymbol{C}^{-1} \tag{6}$$

$$\mathbb{C}_{\text{iso}} = \mathbb{P} : \bar{\mathbb{C}} : \mathbb{P}^t + \frac{2}{3} J^{-\frac{2}{3}} \left[\bar{\boldsymbol{S}} : \boldsymbol{C} \right] \bar{\mathbb{P}} - \frac{2}{3} \left[\boldsymbol{C}^{-1} \otimes \boldsymbol{S}_{\text{iso}} + \boldsymbol{S}_{\text{iso}} \otimes \boldsymbol{C}^{-1} \right] \tag{7}$$

whereas the fictitious tangent operator $\bar{\mathbb{C}}$, the modified projection tensor $\bar{\mathbb{P}}$ and the tensor product $\odot$ are introduced as follows:

$$\bar{\mathbb{C}} = 2J^{-\frac{4}{3}} \frac{\partial \bar{\boldsymbol{S}}}{\partial \bar{\boldsymbol{C}}} = 4J^{-\frac{4}{3}} \frac{\partial^2 \Psi(\bar{\boldsymbol{C}})}{\partial \bar{\boldsymbol{C}}^2} \tag{8}$$

$$\bar{\mathbb{P}} = \boldsymbol{C}^{-1} \odot \boldsymbol{C}^{-1} - \frac{1}{3} \boldsymbol{C}^{-1} \otimes \boldsymbol{C}^{-1} \tag{9}$$

$$\boldsymbol{A} \odot \boldsymbol{B} = -\frac{1}{2} \left[A_{ik} B_{jl} + A_{il} B_{jk} \right]. \tag{10}$$

From equations (4)-(7), stress tensors and tangent operators can be calculated for arbitrary strain energy functions which will later be applied to the different micro-mechanical chain models in Section 4.

2.2 Stress tensor and tangent operator derivation for invariant based models

The general derivation of stress tensors and tangent operators is now particularised for the case of models formulated in terms of strain invariants, i.e. we consider $\Psi = \Psi(I_1, I_2, I_3)$ with $I_i = I_i(\boldsymbol{C})$, $i = 1, 2, 3$ as given in Section 1. For the evaluation of the performance that the models attain in reproducing Treloar's data it will later be of particular interest that the invariants of $\boldsymbol{C}$ are related to the principal stretches λ_i by

$$I_1 = \lambda_1^2 + \lambda_2^2 + \lambda_3^2 \quad , \quad I_2 = \lambda_1^2\lambda_2^2 + \lambda_2^2\lambda_3^2 + \lambda_1^2\lambda_3^2 \quad , \quad I_3 = \lambda_1^2\lambda_2^2\lambda_3^2. \tag{11}$$

Since $\bar{\boldsymbol{C}} = J^{-2/3}\boldsymbol{C}$, the invariants of $\bar{\boldsymbol{C}}$ and $\boldsymbol{C}$ are related by

$$\bar{I}_1 = J^{-2/3} I_1 \quad , \quad \bar{I}_2 = J^{-4/3} I_2 \quad , \quad \bar{I}_3 = \det\left(J^{-2/3}\boldsymbol{C}\right) = J^{-2}\det\boldsymbol{C} = J^{-2} I_3 = 1, \tag{12}$$

i.e. they coincide for the case of incompressibility $J = 1$ and the third invariant then does not at all contribute to the isochoric strain energy. To be able to just reuse the equations for stress tensor and tangent operator summarised in the previous subsection, volumetric-isochoric strain energy decomposition (2) is again assumed and it is sufficient to determine fictitious stress tensor $\bar{\boldsymbol{S}} = 2\partial\Psi_{\text{iso}}/\partial\bar{\boldsymbol{C}}$ and tangent operator $\overline{\mathbb{C}} = 4\partial^2\Psi_{\text{iso}}/\partial\bar{\boldsymbol{C}}\partial\bar{\boldsymbol{C}}$, now from an isochoric strain energy function formulated in terms of the invariants of the isochoric right Cauchy-Green tensor $\bar{\boldsymbol{C}}$, i.e.

$$\Psi_{\text{iso}} = \Psi_{\text{iso}}\left(\bar{I}_1(\bar{\boldsymbol{C}}), \bar{I}_2(\bar{\boldsymbol{C}})\right). \tag{13}$$

Since $\partial\,\text{tr}(\boldsymbol{A})/\partial\boldsymbol{A} = \boldsymbol{I}$ and $\partial\,\text{tr}(\boldsymbol{A}^2)/\partial\boldsymbol{A} = 2\boldsymbol{A}^t$ hold for any second order tensor, the chain rule yields for the fictitious stress tensor:

$$\bar{\boldsymbol{S}} = 2\left[\frac{\partial\Psi_{\text{iso}}}{\partial\bar{I}_1}\frac{\partial\bar{I}_1}{\partial\bar{\boldsymbol{C}}} + \frac{\partial\Psi_{\text{iso}}}{\partial\bar{I}_2}\frac{\partial\bar{I}_2}{\partial\bar{\boldsymbol{C}}} \right] = 2\frac{\partial\Psi_{\text{iso}}}{\partial\bar{I}_1}\boldsymbol{I} + 2\frac{\partial\Psi_{\text{iso}}}{\partial\bar{I}_2}\left[\bar{I}_1\boldsymbol{I} - \bar{\boldsymbol{C}}\right], \quad \text{i.e.}$$

$$\bar{\boldsymbol{S}} = \bar{\gamma}_1\boldsymbol{I} + \bar{\gamma}_2\bar{\boldsymbol{C}} \quad \text{with} \quad \bar{\gamma}_1 = 2\left[\frac{\partial\Psi_{\text{iso}}}{\partial\bar{I}_1} + \bar{I}_1\frac{\partial\Psi_{\text{iso}}}{\partial\bar{I}_2} \right] \quad \text{and} \quad \bar{\gamma}_2 = -2\frac{\partial\Psi_{\text{iso}}}{\partial\bar{I}_2}. \tag{14}$$

The corresponding fictitious tangent operator can be derived from this according to equation (8) and, after some lengthy calculations omitted here, one obtains:

$$\bar{\mathbb{C}} = 2J^{-\frac{4}{3}}\frac{\partial\bar{\boldsymbol{S}}}{\partial\bar{\boldsymbol{C}}} = J^{-\frac{4}{3}}\left[\bar{\delta}_1\boldsymbol{I}\otimes\boldsymbol{I} + \bar{\delta}_2\left[\boldsymbol{I}\otimes\bar{\boldsymbol{C}} + \bar{\boldsymbol{C}}\otimes\boldsymbol{I}\right] + \bar{\delta}_3\bar{\boldsymbol{C}}\otimes\bar{\boldsymbol{C}} + \bar{\delta}_4\mathbb{I}\right], \quad \text{where} \tag{15}$$

$$\bar{\delta}_1 = 4\left[\frac{\partial^2\Psi_{\rm iso}}{\partial\bar{I}_1\partial\bar{I}_1} + 2\bar{I}_1\frac{\partial^2\Psi_{\rm iso}}{\partial\bar{I}_1\partial\bar{I}_2} + \frac{\partial\Psi_{\rm iso}}{\partial\bar{I}_2} + \bar{I}_1^2\frac{\partial^2\Psi_{\rm iso}}{\partial\bar{I}_2\partial\bar{I}_2}\right],$$
$$\bar{\delta}_2 = -4\left[\frac{\partial^2\Psi_{\rm iso}}{\partial\bar{I}_1\partial\bar{I}_2} + \bar{I}_1\frac{\partial^2\Psi_{\rm iso}}{\partial\bar{I}_2\partial\bar{I}_2}\right],$$
$$\bar{\delta}_3 = 4\frac{\partial^2\Psi_{\rm iso}}{\partial\bar{I}_2\partial\bar{I}_2},$$
$$\bar{\delta}_4 = -4\frac{\partial\Psi_{\rm iso}}{\partial\bar{I}_2}.$$

3 Phenomenological models: Stress tensors, tangent operators and performance

Within continuum mechanics, the majority of phenomenological treatments of the elastic behaviour of rubber-like materials depart from the assumption of isotropic hyperelasticity, i.e. a strain energy function usually dependent on the deformation via principal stretches λ_i or strain invariants $I_i = I_i(\boldsymbol{C})$ is considered. Accordingly, phenomenological models are classified into *principal stretch based* and *invariant based models*.

This section reviews ten selected models of this type (cf. Figure 1), provides the corresponding strain energy functions as known from the literature and derives stress tensors and tangent operators according to the equations summarised in the previous section. Furthermore, thermodynamical consistency of all tangent operators is demonstrated by applying a local convergence check (cf. Appendix B) showing that quadratic convergence is ensured when nonlinear boundary value problems are solved by iterative finite-element schemes like Newton-Raphson.

To verify and validate the models, i.e. to evaluate their performance, we resort to the classical experimental Treloar data [1] for the three homogeneous deformation modes uniaxial and equibiaxial tension and pure shear. First, some general details are stated on how to derive analytical stress-stretch relations for these deformation modes for a particular constitutive model. With this at hand, optimal material parameters for each model and deformation mode are determined (*verification*) by a standard fitting procedure. The *validity* of the models is quantified by calculating the errors that arise if the two deformation modes not used for parameter identification are simulated using the fitted parameters.

3.1 Analytical stress formulations for uniaxial tension, equibiaxial tension and pure shear

The Treloar data used here to evaluate the performance of the polymer models are given in pairs of principal stretches λ_i and principal nominal stresses P_i for the three cases of uniaxial and equibiaxial tension and pure shear, cf. Appendix A. To determine optimal material parameters for each model and deformation mode by a standard fitting procedure it is necessary to derive analytical $P_i(\lambda_i)$-formulations from the particular free energy functions. The material investigated by Treloar can be characterised as isotropic and incompressible, a case for which principal stretches and nominal stresses are related by

$$P_i = \frac{\partial\Psi}{\partial\lambda_i} - \frac{1}{\lambda_i}p \quad , \quad i = 1,2,3. \tag{16}$$

The details on how to derive this equation can be found e.g. in [42], [4] or [55]. In case of invariant based models, i.e. $\Psi = \Psi(I_1, I_2)$, the chain rule provides

$$P_i = \frac{\partial\Psi}{\partial I_1}\frac{\partial I_1}{\partial\lambda_i} + \frac{\partial\Psi}{\partial I_2}\frac{\partial I_2}{\partial\lambda_i} - \frac{1}{\lambda_i}p \quad , \quad i = 1,2,3, \tag{17}$$

which subsequently serves to derive the desired analytical formulations for the three deformation modes.

3.1.1 Uniaxial tension (UT)

In uniaxial tension the specimen is elongated in only one direction, e.g. $\lambda_1 = \lambda$. From incompressibility, i.e. $I_3 = \lambda_1^2\lambda_2^2\lambda_3^2 = 1$, and the assumption of isotropy the complementary principal stretches follow as

$\lambda_2 = \lambda_3 = \lambda^{-1/2}$. Thus, the corresponding deformation gradient and the invariants, cf. Eq. (11), are

$$\boldsymbol{F}^{UT} = \begin{bmatrix} \lambda & 0 & 0 \\ 0 & \lambda^{-1/2} & 0 \\ 0 & 0 & \lambda^{-1/2} \end{bmatrix} \quad , \quad I_1^{UT} = 2\lambda^{-1} + \lambda^2 \quad , \quad I_2^{UT} = \lambda^{-2} + 2\lambda. \tag{18}$$

Since the contraction is unhindered in the transversal directions, both $P_{2,3}^{UT}$ are zero and only $P_1^{UT}(\lambda)$ has to be determined. By setting Eq. (17) to zero, e.g. for $i = 2$, and calculating the derivatives $\partial I_{1,2}/\partial\lambda_2$ from Eq. (11), the resultant pressure is determined as

$$p^{UT} = \frac{2}{\lambda}\frac{\partial\Psi}{\partial I_1} + 2\left[\lambda + \frac{1}{\lambda^2}\right]\frac{\partial\Psi}{\partial I_2}. \tag{19}$$

Inserting this into Eq. (17) for $i = 1$, we obtain the analytical formulation for the first principal stress:

$$P_1^{UT} = 2\left[\frac{\partial\Psi}{\partial I_1} + \frac{1}{\lambda}\frac{\partial\Psi}{\partial I_2}\right]\left[\lambda - \frac{1}{\lambda^2}\right]. \tag{20}$$

3.1.2 Equibiaxial tension (ET)

The specimen is equally stretched in two orthogonal directions, i.e. $\lambda_1 = \lambda_2 = \lambda$. Again due to incompressibility, the remaining principal stretch reads $\lambda_3 = \lambda^{-2}$ and the corresponding deformation gradient and invariants follow as

$$\boldsymbol{F}^{ET} = \begin{bmatrix} \lambda & 0 & 0 \\ 0 & \lambda & 0 \\ 0 & 0 & \lambda^{-2} \end{bmatrix} \quad , \quad I_1^{ET} = \lambda^{-4} + 2\lambda^2 \quad , \quad I_2^{ET} = 2\lambda^{-2} + \lambda^4. \tag{21}$$

The stresses in load directions are equal while the third direction is stress-free due to unhindered contraction, i.e. $P_1^{ET} = P_2^{ET}$ and $P_3^{ET} = 0$, respectively. The pressure is determined by setting Eq. (17) to zero for $i = 3$:

$$p^{ET} = \frac{2}{\lambda^4}\frac{\partial\Psi}{\partial I_1} + \frac{4}{\lambda^2}\frac{\partial\Psi}{\partial I_2} \tag{22}$$

and by reinserting this into (17) for $i = 1$ we obtain the first and second principal stresses:

$$P_1^{ET} = P_2^{ET} = 2\left[\frac{\partial\Psi}{\partial I_1} + \lambda^2\frac{\partial\Psi}{\partial I_2}\right]\left[\lambda - \frac{1}{\lambda^5}\right]. \tag{23}$$

3.1.3 Pure shear (PS)

The pure shear setup of Treloar [54] utilises rectangular sheets having a much larger width than length to realise a zero deformation perpendicular to the loading direction $\lambda_1 = \lambda$, i.e. $\lambda_2 = 1$ holds almost everywhere except for the vicinity of the free edges. From incompressibility, the third principal stretch $\lambda_3 = \lambda^{-1}$ and the corresponding deformation gradient and the invariants read

$$\boldsymbol{F}^{PS} = \begin{bmatrix} \lambda & 0 & 0 \\ 0 & 1 & 0 \\ 0 & 0 & \lambda^{-1} \end{bmatrix} \quad , \quad I^{PS} = I_1^{PS} = I_2^{PS} = \lambda^2 + \lambda^{-2} + 1. \tag{24}$$

From unhindered contraction in the third direction the pressure follows from setting (17) to zero for $i = 3$:

$$p^{PS} = \frac{2}{\lambda^2}\frac{\partial\Psi}{\partial I_1} + 2\left[1 + \frac{1}{\lambda^2}\right]\frac{\partial\Psi}{\partial I_2}. \tag{25}$$

Insertion of (25) into (17) yields the principal stresses in load direction and perpendicular to this:

$$P_1^{PS} = 2\left[\frac{\partial\Psi}{\partial I_1} + \frac{\partial\Psi}{\partial I_2}\right]\left[\lambda - \frac{1}{\lambda^3}\right] \tag{26}$$

$$P_2^{PS} = 2\left[\frac{\partial\Psi}{\partial I_1} + \lambda^2\frac{\partial\Psi}{\partial I_2}\right]\left[1 - \frac{1}{\lambda^2}\right]. \tag{27}$$

3.2 Models formulated in principal stretches: Ogden models (1972)

A sophisticated class of models frequently used for the simulation of rubber-like materials goes back to Ogden [10]. Although markedly modular and flexible it is known that the determination of its material parameters may become difficult if more complex versions are utilised [20]. The free energy density is formulated as a finite sum of scaled powers of the principal stretches λ_i, which are the square roots of the eigenvalues of the right Cauchy-Green tensor $\boldsymbol{C}$, i.e. $\lambda_i^2 \boldsymbol{N}_i = \boldsymbol{C} \cdot \boldsymbol{N}_i$, $i = 1, 2, 3$. The eigenvectors $\boldsymbol{N}_i$ are also referred to as principal referential directions. With regard to additive decomposition (2) we consider the following isochoric free energy density

$$\Psi_{\text{iso}} = \sum_{k=1}^{K} \frac{\mu_k}{\alpha_k} \left[\bar{\lambda}_1^{\alpha_k} + \bar{\lambda}_2^{\alpha_k} + \bar{\lambda}_3^{\alpha_k} - 3 \right] \tag{28}$$

in terms of the modified principal stretches $\bar{\lambda}_i = J^{-1/3} \lambda_i$, the square roots of the eigenvalues of $\bar{\boldsymbol{C}}$. Model (28) is adjustable by $2K$ material parameters, the shear modulus like μ_k and the dimensionless exponents α_k, for which a consistency condition can be derived from comparison with the linear theory: $\sum_k \mu_k \alpha_k = 2\mu$, wherein μ is the classical shear modulus, and $\mu_k \alpha_k > 0$ have to be satisfied.

Models formulated in principal stretches intrinsically require to solve the eigenvalue problem of the considered strain tensor. From the eigenvalues the corresponding eigenbasis $\{\boldsymbol{N}_1, \boldsymbol{N}_2, \boldsymbol{N}_3\}$ for the spectral representation $\bar{\boldsymbol{C}} = \sum \bar{\lambda}_i^2 \, \boldsymbol{N}_i \otimes \boldsymbol{N}_i$ can be determined, e.g. by Serrin's formula. Since eigenbases of stress and strain coincide for isotropic materials, the format of the stress tensor follows straightforward as

$$\boldsymbol{S}_{\text{iso}} = \sum_{i=1}^{3} S_{\text{iso}}^i \, \boldsymbol{N}_i \otimes \boldsymbol{N}_i \tag{29}$$

and only necessitates the computation of the eigenvalues S_{iso}^i. Due to the fact that Ψ_{iso} does not directly depend on $\bar{\boldsymbol{C}}$, it provides no further advantage to use fictitious stress $\bar{\boldsymbol{S}}$ and the corresponding projection operators, cf. Eqns. (5)-(9), to compute $\boldsymbol{S}_{\text{iso}}$ and $\mathbb{C}_{\text{iso}}$ but to start immediately from Eq. (3). Recalling that $\partial \lambda_i^2 / \partial \boldsymbol{C} = \boldsymbol{N}_i \otimes \boldsymbol{N}_i$ in case of three distinct eigenvalues, the chain rule applied to equation $(3)_1$ yields

$$\boldsymbol{S}_{\text{iso}} = 2 \frac{\partial \Psi_{\text{iso}}(\bar{\lambda}_i)}{\partial \boldsymbol{C}} = 2 \sum_{i=1}^{3} \frac{\partial \Psi_{\text{iso}}}{\partial \lambda_i^2} \frac{\partial \lambda_i^2}{\partial \boldsymbol{C}} = \sum_{i=1}^{3} \frac{1}{\lambda_i} \frac{\partial \Psi_{\text{iso}}}{\partial \lambda_i} \boldsymbol{N}_i \otimes \boldsymbol{N}_i \,, \tag{30}$$

i.e. $S_{\text{iso}}^i = \lambda_i^{-1} \partial \Psi_{\text{iso}} / \partial \lambda_i$ from comparing coefficients with (29). This can be resolved further by exploiting $\partial \bar{\lambda}_i / \partial \lambda_j = J^{-1/3} [\delta_{ij} - \frac{1}{3} \bar{\lambda}_i \bar{\lambda}_j^{-1}]$ and, after some algebraic manipulations and insertion of $\partial(28)/\partial \bar{\lambda}_i$, the eigenvalues completing spectral representation (29) of the isochoric stress tensor follow as

$$S_{\text{iso}}^i = J^{-2/3} \left[\sum_{k=1}^{K} \mu_k \bar{\lambda}_i^{\alpha_k - 2} - \sum_{j=1}^{3} \sum_{k=1}^{K} \frac{\mu_k}{3} \frac{\bar{\lambda}_j^{\alpha_k}}{\bar{\lambda}_i^2} \right] \,, \; i = 1, 2, 3. \tag{31}$$

Concerning a detailed derivation of the corresponding spectral representation of the isochoric tangent operator $\mathbb{C}_{\text{iso}}$ the interested reader is referred to [42], [51] or [61]:

$$\mathbb{C}_{\text{iso}} = \sum_{i,j=1}^{3} \frac{1}{\lambda_j} \frac{\partial S_{\text{iso}}^i}{\partial \lambda_j} \boldsymbol{N}_i \otimes \boldsymbol{N}_i \otimes \boldsymbol{N}_j \otimes \boldsymbol{N}_j + \sum_{\substack{i,j=1 \\ i \neq j}}^{3} \frac{S_{\text{iso}}^j - S_{\text{iso}}^i}{\lambda_j^2 - \lambda_i^2} \left[\boldsymbol{N}_i \otimes \boldsymbol{N}_j \otimes \boldsymbol{N}_i \otimes \boldsymbol{N}_j + \boldsymbol{N}_i \otimes \boldsymbol{N}_j \otimes \boldsymbol{N}_j \otimes \boldsymbol{N}_i \right]. \tag{32}$$

Here, only the derivatives $\partial S_{\text{iso}}^i / \partial \lambda_j$ within the first sum term remain to be computed from Eq. (31). To demonstrate the thermodynamical consistency of tangent operator (32) we employ the local convergence test explained in Appendix B, which iteratively determines the strain tensor that corresponds to a prescribed stress tensor for a certain set of material parameters. By choosing the parameter set published in [42] for Treloar's uniaxial elastomer data, i.e. $[\mu_1, \mu_2, \mu_3] = [0.63, 0.0012, -0.01]$ MPa, $[\alpha_1, \alpha_2, \alpha_3] = [1.3, 5.0, -2.0]$, the local test converges quadratically to $\boldsymbol{C}_\infty = [1.51, 2.62, 1.28, 1.59, 0.0, 0.0]$, as is indicated by the evolutions of the Euclidean norms of residuals and strain updates:

Iteration n	0	1	2	3	4
$\|\boldsymbol{R}(\boldsymbol{C}_n)\|_2$	2.01e-01	5.24e-01	4.15e-03	1.08e-05	3.46e-12
$\|\boldsymbol{C}_{n+1} - \boldsymbol{C}_n\|_2$	2.03e-01	3.56e-02	1.809e-03	2.1e-06	1.06e-12

Analytical $P_i(\lambda_i)$-relations for the deformation modes UT, ET and PS, which are required to check the performance of the model on Treloar's data, can be derived from (16) together with free energy density (28). In analogy to Sections 3.1.1-3.1.3, the pressure p has to be determined beforehand from the respective boundary conditions, i.e. from evaluating Eq. (16) for $P_i = 0$. The resulting stress-stretch relations read

$$P_1^{UT} = \sum_{k=1}^{K} \mu_k^{UT} \left[\lambda^{\alpha_k^{UT}-1} - \lambda^{-\frac{1}{2}\alpha_k^{UT}-1} \right], \tag{33}$$

$$P_{1,2}^{ET} = \sum_{k=1}^{K} \mu_k^{ET} \left[\lambda^{\alpha_k^{ET}-1} - \lambda^{-2\alpha_k^{ET}-1} \right], \tag{34}$$

$$P_1^{PS} = \sum_{k=1}^{K} \mu_k^{PS} \left[\lambda^{\alpha_k^{PS}-1} - \lambda^{-\alpha_k^{PS}-1} \right], \tag{35}$$

whereas λ denotes the isochoric stretch in the corresponding load direction as given in the previous subsections. Note that only the coefficients to α_k differ between the deformation modes. By using Matlab's Curve Fitting Toolbox, Equations (33)-(35) are now fitted to the corresponding Treloar data (cf. Appendix A) to obtain optimal parameters for the three increasingly complex Ogden models with $K = 1, 2, 3$:

$K = 1$		
$\mu_1^{UT} = 0.01668$	$\mu_1^{ET} = 0.2958$	$\mu_1^{PS} = 0.3105$
$\alpha_1^{UT} = 3.854$	$\alpha_1^{ET} = 2.366$	$\alpha_1^{PS} = 2.062$
$K = 2$		
$\boldsymbol{\mu}^{UT} =$ [0.3055,2.316e-6]	$\boldsymbol{\mu}^{ET} =$ [0.4856,1.965e-3]	$\boldsymbol{\mu}^{PS} =$ [0.4726,1.256e-3]
$\boldsymbol{\alpha}^{UT} =$ [1.996,8.022]	$\boldsymbol{\alpha}^{ET} =$ [1.659,5.268]	$\boldsymbol{\alpha}^{PS} =$ [1.57,4.869]
$K = 3$		
$\boldsymbol{\mu}^{UT} =$ [0.5649,3.856e-3,5.7e-13]	$\boldsymbol{\mu}^{ET} =$ [0.4848,1.918e-3,2.8e-14]	$\boldsymbol{\mu}^{PS} =$ [0.557,1.947e-2,1.3e-11]
$\boldsymbol{\alpha}^{UT} =$ [1.297,4.342,15.13]	$\boldsymbol{\alpha}^{ET} =$ [1.662,5.281,2.1e-9]	$\boldsymbol{\alpha}^{PS} =$ [1.231,3.413,15]

Comparing UT-parameters for $K = 3$ with those from [42] cited above reveals significant qualitative and quantitative differences – even though the experimental data are reproduced almost perfectly by both parameter sets, see Fig. 4 (left). These discrepancies are explicable by the high flexibility of large-K Ogden models whose increasing number of parameters simultaneously produces a severe sensitivity of the optimisation method wrt the initial values. In particular, one can observe that the fitting procedure optimises certain parameters close to zero, i.e. it reduces the complexity of the model by switching off certain terms. This behaviour reflects a general problem reported also by other authors: reliable parameter identification becomes more difficult the more flexible the considered models are. Consequently, an ideal model should not exceed the complexity of the material behaviour it has to capture, which is important especially in designing phenomenological models since these usually abdicate a direct relation to the causative material structure.

To validate the models, each set of optimal material parameters for UT, ET and PS is now used to compute the response of the other two deformation modes. The results are plotted in Figs. 2-4 which additionally contain the errors between (a) each experiment and its optimal fit, e.g. Error(UT-fit), and (b) the simulations of the other deformation modes and their respective measurements, e.g. Error(ET-sim). All errors are calculated according to

$$\text{Error(fit/sim)} = \sqrt{\frac{1}{N} \sum_{i=1}^{N} \left[P_{\text{fit/sim}}(\lambda_i^{\text{Treloar}}) - P_{\text{Treloar}}(\lambda_i^{\text{Treloar}}) \right]^2}, \tag{36}$$

i.e. sum up the squared differences between fitted/simulated and measured stresses, respectively, averaged by the number of data points N (stretches) available for each deformation mode.

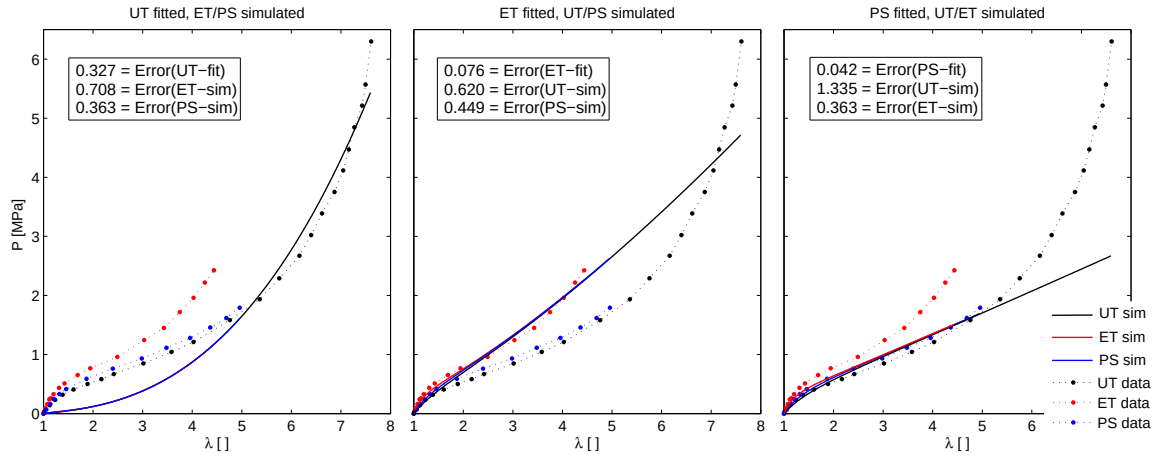

Fig. 2 Performance of the simplest Ogden model ($K = 1$) on the Treloar data. Both fitting quality and generalisation, i.e. the capability to correctly simulate deformation modes not used for optimisation, are rather poor since this two parameter model cannot change its curvature. Furthermore, all stress-stretch relations yield almost identical curves for a certain parameter set.

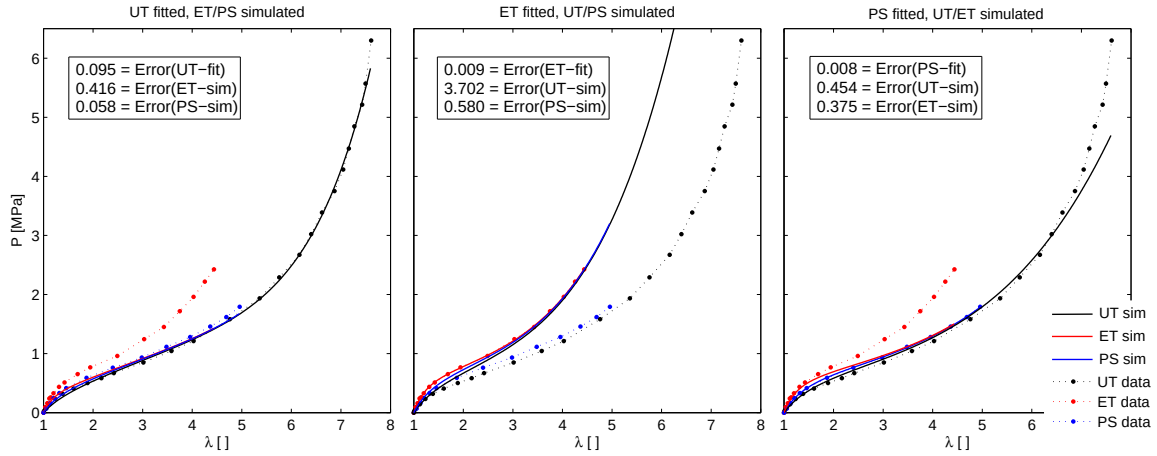

Fig. 3 Performance of the Ogden model with $K = 2$ on the Treloar data. The fitting quality is acceptable (UT) to perfect (ET,PS), but the generalisation still is not sufficient since the small differences between the three stress-stretch relations do not impose curves significantly differing for a particular parameter set.

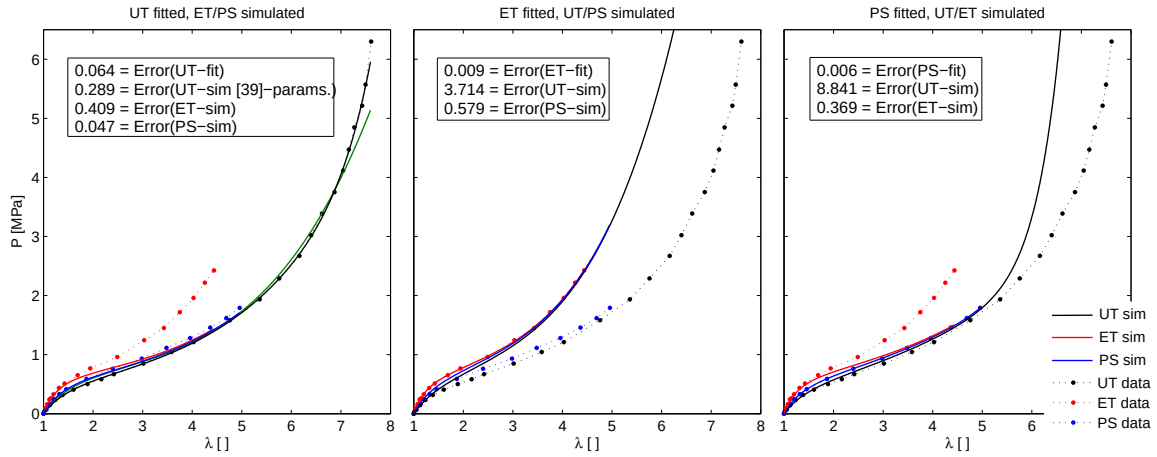

Fig. 4 Performance of the Ogden model with $K = 3$ on the Treloar data. The fitting quality is close to perfection, the generalisation is slightly better than for $K = 2$ but still far from satisfactorily. For comparison, the left figure also contains a UT-simulation (green line) using the parameters published in [42].

3.3 Models formulated in strain invariants

For the most general case, one can assume a strain energy function depending on the invariants of the right Cauchy-Green tensor, i.e. $\Psi = \Psi(I_1(\boldsymbol{C}), I_2(\boldsymbol{C}), I_3(\boldsymbol{C}))$, which is continuously differentiable with respect to all I_i. Then, this strain energy function Ψ can be expanded in an infinite Taylor series of the form

$$\Psi = \Psi(I_1, I_2, I_3) = \sum_{k,l,m=0}^{\infty} c_{klm} \left[I_1 - 3\right]^k \left[I_2 - 3\right]^l \left[I_3 - 1\right]^m , \tag{37}$$

where c_{klm} denote material parameters. The above form is termed as the general form of the Mooney-Rivlin strain energy function [52],[53]. In case of incompressible material behaviour, $\det(\boldsymbol{F}) = \lambda_1\lambda_2\lambda_3 = J = 1$ and, thus, $I_3 = \det(\boldsymbol{C}) = \det(J^{2/3}\bar{\boldsymbol{C}}) = \det(\bar{\boldsymbol{C}}) = \bar{I}_3 = 1$ and the invariants I_i of $\boldsymbol{C}$ coincide with the invariants $\bar{I}_i$ of the isochoric right Cauchy-Green tensor $\bar{\boldsymbol{C}}$. Consequently, equation (37) can be reduced to the isochoric strain energy function:

$$\Psi_{\text{iso}} = \Psi_{\text{iso}}(I_1(\boldsymbol{C}), I_2(\boldsymbol{C})) = \Psi_{\text{iso}}\big(\bar{I}_1(\bar{\boldsymbol{C}}), \bar{I}_2(\bar{\boldsymbol{C}})\big) = \sum_{k,l=0}^{\infty} c_{kl} \left[\bar{I}_1 - 3\right]^k \left[\bar{I}_2 - 3\right]^l . \tag{38}$$

This equation provides the foundation for all invariant based models, some of which are reviewed in the following subsections. Every invariant based model can, due to Eqn. (11), be reformulated as a principal stretch based model, while the inverse transformation is not necessarily possible.

3.3.1 Neo-Hooke model (1943)

The Neo-Hooke model constitutes the simplest specification of the Mooney-Rivlin model series since it only considers $c_{10} \neq 0$ in equation (38), i.e. the summation stops at $k = 1$, $l = 0$ and the additive constant c_{00} is set to zero. The resulting isochoric free energy function reads

$$\Psi_{\text{iso}} = \frac{\mu}{2} \left[\bar{I}_1 - 3\right] , \tag{39}$$

where the only material parameter $\mu = 2c_{10}$ denotes the shear modulus. This model coincides with the 3-chain model, cf. Section 4.1, which is a micro-mechanically motivated ansatz that uses Gaussian chains oriented along the principal stretch directions. Evaluation of Eqns. (14) and (15) provides the corresponding fictitious stress tensor and tangent operator:

$$\bar{\boldsymbol{S}} = \mu \boldsymbol{I} \tag{40}$$

$$\bar{\mathbb{C}} = \boldsymbol{0} \otimes \boldsymbol{0}. \tag{41}$$

Note that only the fictitious tangent operator is zero here, the complete tangent according to Eqns. (6),(7) is non-zero. For $\mu = 0.5673$ MPa, the local convergence test introduced in Appendix B quadratically converges to $\boldsymbol{C}_\infty = [1.58, 2.46, 1.22, 1.53, 0.0, 0.0]$, as is indicated by the evolutions of the Euclidean norms of residuals and strain updates:

Iteration n	0	1	2	3	4
$\left\|\boldsymbol{R}(\boldsymbol{C}_n)\right\|_2$	4.49e-01	3.04e-01	3.89e-03	2.41e-06	2.27e-13
$\left\|\boldsymbol{C}_{n+1} - \boldsymbol{C}_n\right\|_2$	2.94e-01	5.91e-02	7.78e-04	5.05e-07	3.55e-14

The analytical $P_i(\lambda_i)$-relations for the three deformation modes UT, ET and PS, which are required to check the performance of the model on the Treloar data, are obtained from Eqns. (20), (23), (26) as

$$P_1^{UT} = \mu^{UT} \left[\lambda - \lambda^{-2}\right] \tag{42}$$

$$P_{1,2}^{ET} = \mu^{ET} \left[\lambda - \lambda^{-5}\right] \tag{43}$$

$$P_1^{PS} = \mu^{PS} \left[\lambda - \lambda^{-3}\right] . \tag{44}$$

Fitting each of these equations to the corresponding Treloar data (cf. Appendix A) yields the following optimal material parameters:

$$\mu^{UT} = 0.5673 \text{ MPa} \quad , \quad \mu^{ET} = 0.4104 \text{ MPa} \quad , \quad \mu^{PS} = 0.336 \text{ MPa}. \tag{45}$$

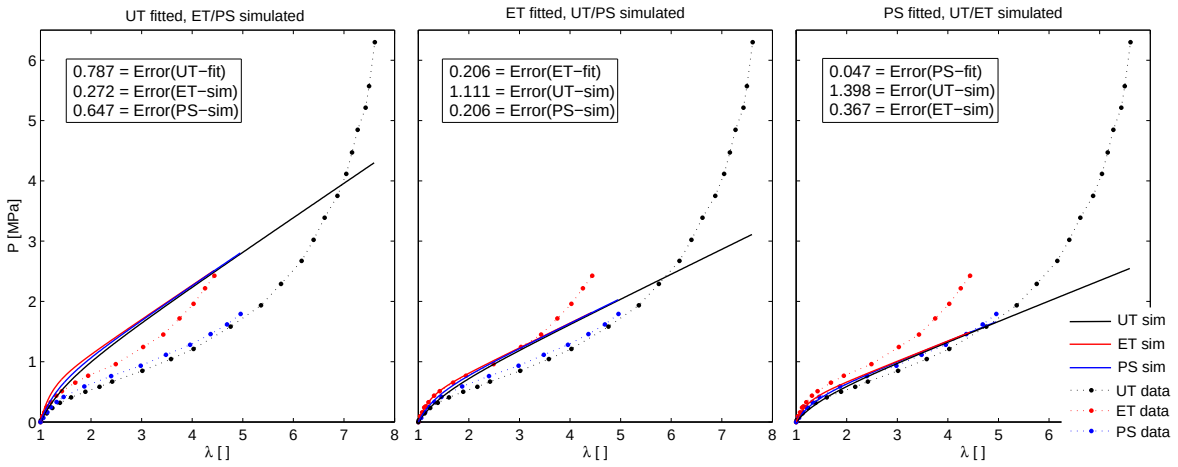

Fig. 5 Performance of the neo-Hooke model on the Treloar data. The minimum least squares fits to UT **(left)** and ET **(middle)** yield inacceptable results due to the incapability of the model to reproduce the S-shape. The latter is less dominant for PS **(right)**, which leads to an acceptable fit quality in this case. Using the optimal parameter of a certain deformation mode to simulate different modes is not advisable, as is indicated by the error values.

Each of these optimal material parameters is now used to simulate the experimental data of the other two deformation modes. The results are plotted in Fig. 5, which additionally gives the errors that occur from the fitting procedure and the simulation of the experiments that have not been used for parameter identification. Obviously, the neo-Hookean ansatz is not sufficient to correctly reproduce the experimental data. Especially the characteristic S-shape cannot be captured since the simple model structure does not allow for a change of curvature. Merely fitting the PS-data yields an acceptable result. Nonetheless, if only small deformations below 50% stretch are considered, the neo-Hooke model provides reasonable results, cf. also [56].

3.3.2 Mooney-Rivlin model (1940)

A more sophisticated, yet simple specification of equation (38) is called Mooney-Rivlin or Mooney model. It considers $c_{10} \neq 0 \neq c_{01}$, i.e. the summation stops at $k, l = 1$ and c_{00}, c_{11} are set to zero. This ansatz can also be classified as a model of Ogden type, cf. e.g. [42] for the corresponding formulation in terms of principal stretches. Its main advantage compared to the neo-Hooke model is the consideration of the second invariant:

$$\Psi_{\text{iso}} = c_{10}\left[\bar{I}_1 - 3\right] + c_{01}\left[\bar{I}_2 - 3\right]. \tag{46}$$

Here, $2c_{10} =: \mu_1$ and $2c_{01} =: -\mu_2$ denote material parameters of shear modulus type which are related to the standard shear modulus via $\mu = \mu_1 - \mu_2$. Again, evaluation of Eqns. (14) and (15) provides the corresponding fictitious stress tensor and tangent operator:

$$\bar{\boldsymbol{S}} = 2\left[c_{10} + c_{01}\bar{I}_1\right]\boldsymbol{I} - 2c_{01}\bar{\boldsymbol{C}} \tag{47}$$

$$\bar{\mathbb{C}} = 4J^{-\frac{4}{3}}\left[c_{01}\boldsymbol{I}\otimes\boldsymbol{I} - c_{01}\mathbb{I}\right]. \tag{48}$$

For $[c_{10}, c_{01}] = [0.2837, 0.0]$ MPa, the local test (Appendix B) quadratically converges to $\boldsymbol{C}_\infty = [1.74, 2.78, 1.18, 1.79, 0.0, 0.0]$, as is indicated by the evolutions of the Euclidean norms of residuals and strain updates:

Iteration n	0	1	2	3	4
$\|\boldsymbol{R}(\boldsymbol{C}_n)\|_2$	4.49e-01	3.04e-01	3.91e-03	2.42e-06	2.48e-13
$\|\boldsymbol{C}_{n+1} - \boldsymbol{C}_n\|_2$	2.95e-01	5.92e-02	7.80e-04	5.07e-07	3.45e-14

The analytical $P_i(\lambda_i)$-relations for the three deformation modes UT, ET and PS, which are required to check the performance of the model on the Treloar data, are obtained from Eqns. (20), (23), (26) as

$$P_1^{UT} = c_{10}^{UT}\left[2\lambda - 2\lambda^{-2}\right] + c_{01}^{UT}\left[2 - 2\lambda^{-3}\right] \tag{49}$$

$$P_{1,2}^{ET} = c_{10}^{ET}\left[2\lambda - 2\lambda^{-5}\right] + c_{01}^{ET}\left[2\lambda^3 - 2\lambda^{-3}\right] \tag{50}$$

$$P_1^{PS} = c_{10}^{PS}\left[2\lambda - 2\lambda^{-3}\right] + c_{01}^{PS}\left[2\lambda - 2\lambda^{-3}\right]. \tag{51}$$

From fitting these equations to the corresponding Treloar data, the following sets of optimal parameters result:

$$c_{10}^{UT} = 0.2837 \text{ MPa} \quad , \quad c_{10}^{ET} = 0.1713 \text{ MPa} \quad , \quad c_{10}^{PS} = 0.1263 \text{ MPa} \tag{52}$$

$$c_{01}^{UT} = 0.0000 \text{ MPa} \quad , \quad c_{01}^{ET} = 0.0047 \text{ MPa} \quad , \quad c_{01}^{PS} = 0.0413 \text{ MPa}. \tag{53}$$

To validate the model, each of these sets is used to simulate the experimental data of the other two deformation modes. The results are plotted in Fig. 6, together with the errors that occur from fitting and simulation of experiments not used for parameter identification. The Mooney-Rivlin model performs satisfactorily on the experimental data up to stretches of $\lambda \leq 4.5$, but only if fitted to equibiaxial data. Pure shear can be reproduced by fitting, but the obtained parameters are not suited for other deformation modes. The model is not complex enough to capture the pronounced S-shape of uniaxial deformations at high strains.

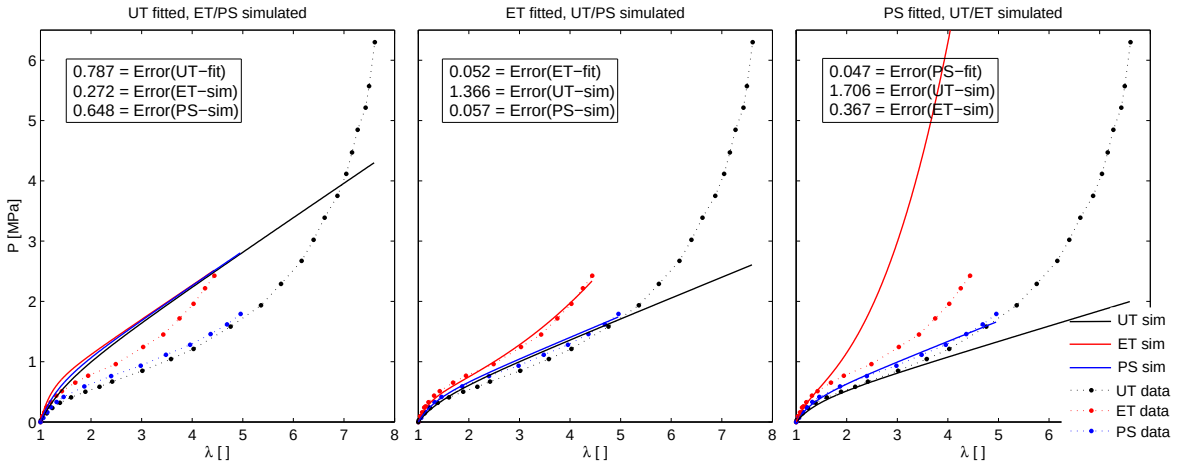

Fig. 6 Performance of the Mooney-Rivlin model on the Treloar data. For UT **(left)** both fitting quality and simulation errors are identically insufficient as for the neo-Hooke model since the term containing the second invariant is not activated. This is not the case for ET **(middle)** where the quality of the fit is quite good and also the simulation of PS and UT yield reasonable results up to strains of 350 %. The optimal parameters for PS **(right)** should not be used, neither for UT nor PS.

3.3.3 Isihara model (1951)

The insufficient reproduction of S-shaped load-deformation curves by most of the earlier elastomer models can, from a molecular point of view, be ascribed to the neglection of the non-Gaussian character in the configurational entropy of a single chain. To overcome this, Isihara et al. [39] proposed a model incorporating a non-Gaussian chain theory. The linearisation of the corresponding equations leads to a formulation of the Mooney-Rivlin series type that contains three material parameters and, most important, a term nonlinearly coupling the two invariants $\bar{I}_1$ and $\bar{I}_2$. The free energy function reads, according to [20]:

$$\Psi_{\text{iso}} = c_{10}\left[\bar{I}_1 - 3\right] + c_{20}\left[\bar{I}_1 - 3\right]^2 c_{01}\left[\bar{I}_2 - 3\right], \tag{54}$$

where c_{10}, c_{20}, c_{01} are the governing material parameters. From Eqns. (14) and (15) fictitious stress tensor and tangent operator are determined as

$$\bar{\boldsymbol{S}} = \left[2c_{10} + 4c_{20}c_{01}\left[\bar{I}_1 - 3\right]\left[\bar{I}_2 - 3\right] + 2c_{20}c_{01}\bar{I}_1\left[\bar{I}_1 - 3\right]^2\right]\boldsymbol{I} - 2c_{20}c_{01}\left[\bar{I}_1 - 3\right]^2\bar{\boldsymbol{C}} \tag{55}$$

$$\bar{\mathbb{C}} = J^{-\frac{4}{3}}\left[\bar{\delta}_1\boldsymbol{I}\otimes\boldsymbol{I} + \bar{\delta}_2\left[\boldsymbol{I}\otimes\bar{\boldsymbol{C}} + \bar{\boldsymbol{C}}\otimes\boldsymbol{I}\right] + \bar{\delta}_3\bar{\boldsymbol{C}}\otimes\bar{\boldsymbol{C}} + \bar{\delta}_4\mathbb{I}\right], \tag{56}$$

with

$$\bar{\delta}_1 = 8c_{20}c_{01}\left[\bar{I}_2 - 3\right] + 16c_{20}c_{01}\bar{I}_1\left[\bar{I}_1 - 3\right] + 4c_{20}c_{01}\left[\bar{I}_1 - 3\right]^2 \tag{57}$$

$$\bar{\delta}_2 = -8c_{20}c_{01}\left[\bar{I}_1 - 3\right] \tag{58}$$

$$\bar{\delta}_3 = 0 \tag{59}$$

$$\bar{\delta}_4 = -4c_{20}c_{01}\left[\bar{I}_1 - 3\right]^2. \tag{60}$$

For $[c_{10}, c_{20}, c_{01}] = [0.1161, 0.0136, 0.0114]$ MPa, the local test (Appendix B) converges quadratically to $\boldsymbol{C}_\infty = [1.58, 2.46, 1.22, 1.53, 0.0, 0.0]$, as is indicated by the evolutions of the Euclidean norms of residuals and strain updates:

Iteration n	0	1	2	3
$\|\boldsymbol{R}(\boldsymbol{C}_n)\|_2$	4.40e-01	1.27e-01	9.93e-04	3.91e-08
$\|\boldsymbol{C}_{n+1} - \boldsymbol{C}_n\|_2$	1.39e-01	1.83e-02	9.42e-05	9.78e-09

The analytical $P_i(\lambda_i)$-relations for UT, ET and PS follow again from Eqns. (20), (23), (26) – together with the here omitted insertion of the corresponding $\bar{I}_{1/2}^{UT/ET/PS}(\lambda)$-terms according to Eqns. (18), (21), (24):

$$P_1^{UT} = \left[2c_{10}^{UT} + 4c_{20}^{UT}c_{01}^{UT}\left[\bar{I}_1^{UT} - 3\right]\left[\bar{I}_2^{UT} - 3\right] + c_{20}^{UT}c_{01}^{UT}\lambda^{-1}\left[\bar{I}_1^{UT} - 3\right]^2\right]\left[\lambda - \lambda^{-2}\right] \tag{61}$$

$$P_{1,2}^{ET} = \left[2c_{10}^{ET} + 4c_{20}^{ET}c_{01}^{ET}\left[\bar{I}_1^{ET} - 3\right]\left[\bar{I}_2^{ET} - 3\right] + c_{20}^{ET}c_{01}^{ET}\lambda^{2}\left[\bar{I}_1^{ET} - 3\right]^2\right]\left[\lambda - \lambda^{-5}\right] \tag{62}$$

$$P_1^{PS} = \left[2c_{10}^{PS} + 6c_{20}^{PS}c_{01}^{PS}\left[\bar{I}^{PS} - 3\right]^2\right]\left[\lambda - \lambda^{-3}\right] \quad \text{since} \quad \bar{I}_1^{PS} = \bar{I}_2^{PS}\,. \tag{63}$$

The following sets of optimal parameters result from fitting these equations to the corresponding Treloar data:

$$c_{10}^{UT} = 0.1161 \text{ MPa} \quad , \quad c_{10}^{ET} = 0.1993 \text{ MPa} \quad , \quad c_{10}^{PS} = 0.1601 \text{ MPa} \tag{64}$$

$$c_{20}^{UT} = 0.0136 \text{ MPa} \quad , \quad c_{20}^{ET} = 0.0015 \text{ MPa} \quad , \quad c_{20}^{PS} = 0.0037 \text{ MPa} \tag{65}$$

$$c_{01}^{UT} = 0.0114 \text{ MPa} \quad , \quad c_{01}^{ET} = 0.0013 \text{ MPa} \quad , \quad c_{01}^{PS} = 0.0031 \text{ MPa}. \tag{66}$$

Each of these sets is again used to simulate the experimental data of the other two deformation modes. The results are plotted in Fig. 7, as well as the corresponding errors from both fitting and the simulation of experiments not used for parameter identification. The fit quality is very high for all deformation modes, especially for ET and PS almost perfect results are obtained. Isihara's model is obviously suited to capture the characteristic S-shape at large deformations. The non-linearity of this model is yet not sufficient to simultaneously reproduce the high initial stiffness and the change in curvature at large stretches, as is reflected by the unsatisfying UT-curve. Furthermore, uniaxial tension is not recommendable to gauge the model for other deformation modes which is due to the dominance of $\bar{I}_1$ in the second term (compare the unphysically high stress increases for ET and PS, Fig. 7, left). The situation is better for the other two cases but from comparison of Fig. 7, middle vs. left part, the impression arises that this model is particularly sensitive to the curvature and the stretch range of the data used for parameter identification.

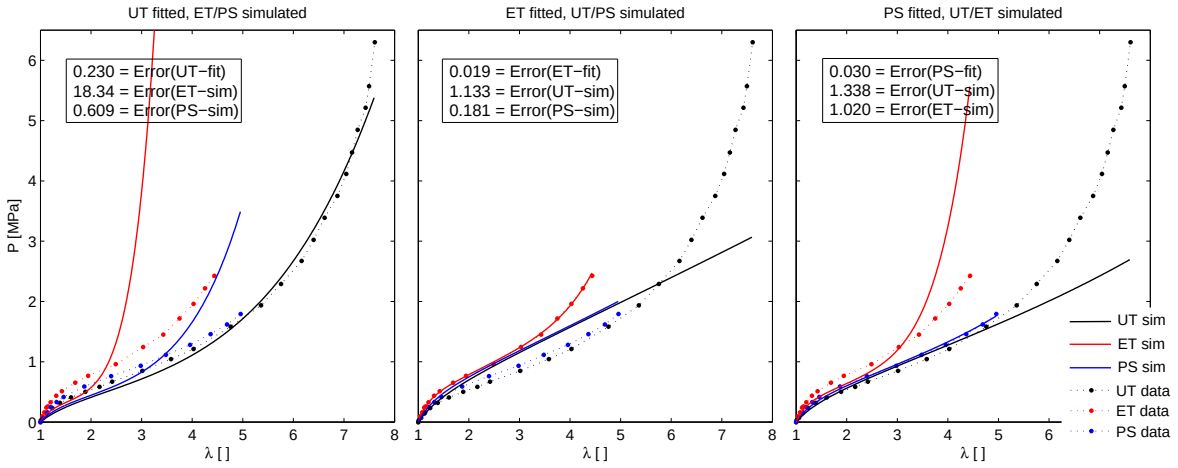

Fig. 7 Performance of the Isihara model on the Treloar data. The model provides low fitting errors for all deformation modes, merely the UT fit **(left)** is not optimal. For both ET **(middle)** and PS **(right)** the very small deviations can probably be ascribed to the non-smoothness of the experimental data. The simulation errors do not allow a final conclusion on the validity of the model.

3.3.4 Gent-Thomas model (1958)

Gent and Thomas [40] proposed another empirical two-parameter model similar to that of Mooney and Rivlin but introducing a scaled logarithm of $\bar{I}_2$. It can be interpreted as a mathematically convenient approximation of a more complex model derived by Thomas [41] from a modified network theory. The corresponding isochoric free energy density is given by

$$\Psi_{\text{iso}} = c_1 \left[\bar{I}_1 - 3\right] + c_2 \ln\left(\frac{\bar{I}_2}{3}\right), \tag{67}$$

wherein c_1, c_2 are denoting material parameters. Fictitious stress tensor and tangent operator follow as

$$\bar{\boldsymbol{S}} = 2\left[c_1 + c_2\frac{\bar{I}_1}{\bar{I}_2}\right]\boldsymbol{I} - 2\frac{c_2}{\bar{I}_2}\bar{\boldsymbol{C}} \tag{68}$$

$$\bar{\mathbb{C}} = 4c_2 J^{-\frac{4}{3}}\left[\frac{1-\bar{I}_2}{\bar{I}_2}\boldsymbol{I}\otimes\boldsymbol{I} + \frac{\bar{I}_1}{\bar{I}_2^2}\left[\boldsymbol{I}\otimes\bar{\boldsymbol{C}} + \bar{\boldsymbol{C}}\otimes\boldsymbol{I}\right] - \frac{1}{\bar{I}_2^2}\bar{\boldsymbol{C}}\otimes\bar{\boldsymbol{C}} - \frac{1}{\bar{I}_2}\mathbb{I}\right] \tag{69}$$

from evaluation of Eqns. (14) and (15). With parameters $[c_1, c_2]$ = [0.2837,2.81e-11] MPa, the local test (Appendix B) quadratically converges to $\boldsymbol{C}_\infty = [1.59, 2.49, 1.22, 1.55, 0.0, 0.0]$, as the following table indicates:

Iteration n	0	1	2	3	4
$\|\boldsymbol{R}(\boldsymbol{C}_n)\|_2$	4.49e-01	3.04e-01	3.91e-03	2.42e-06	2.33e-13
$\|\boldsymbol{C}_{n+1} - \boldsymbol{C}_n\|_2$	2.95e-01	5.92e-02	7.80e-04	5.07e-07	3.39e-14

The analytical $P_i(\lambda_i)$-relations follow from (20), (23), (26) with $\bar{I}_{1,2}^{UT/ET/PS}$ inserted from (18), (21), (24):

$$P_1^{UT} = \frac{2c_1^{UT}[\lambda^3 - 1]}{\lambda^2} + \frac{2c_2^{UT}[\lambda^3 - 1]}{2\lambda^4 + \lambda} \tag{70}$$

$$P_{1,2}^{ET} = \frac{2c_1^{ET}[\lambda^6 - 1]}{\lambda^5} + \frac{2c_2^{ET}[\lambda^6 - 1]}{\lambda^7 + 2\lambda} \tag{71}$$

$$P_1^{PS} = \frac{2c_1^{PS}[\lambda^4 - 1]}{\lambda^3} + \frac{2c_2^{PS}[\lambda^4 - 1]}{\lambda^5 + \lambda^3 + \lambda}. \tag{72}$$

Fitting each of these equations to the corresponding Treloar data yields the following material parameter sets:

$$c_1^{UT} = 0.2837 \text{ MPa} \quad , \quad c_1^{ET} = 0.2052 \text{ MPa} \quad , \quad c_1^{PS} = 0.1629 \text{ MPa} \tag{73}$$

$$c_2^{UT} = 2.81\text{e-}11 \text{ MPa}\,, \quad c_2^{ET} = 2.22\text{e-}14 \text{ MPa}\,, \quad c_2^{PS} = 0.0376 \text{ MPa}\,. \tag{74}$$

Figure 8 depicts the fits, the simulations of complementary deformation modes and the errors wrt to Treloar's data. The reproduction of experimental data as well as the validity of the paramters are almost identical to those of the Neo-Hookean model. Better results can be obtained if the strain range used for optimisation does not require a change in curvature, which the model is unable to capture since higher powers of $\bar{I}_1$ are missing.

3.3.5 Swanson model (1985)

An invariant based model with a structure similar to that of Ogden's series expansion has been proposed by Swanson [43],[44]. Its free energy contains two sums of weighted non-integer powers of the isochoric invariants, thus allowing complexity, i.e. number of parameters, and non-linearity of the model to be arbitrarily adjusted. The major advantage of Swanson's approach is that neither eigenvalues nor -vectors of the strain tensor need to be calculated as in the case of Ogden's model. Nonetheless, due to the fast growing number of parameters similar difficulties in the determination of the material constants have to be expected [37],[56]. The isochoric strain energy function is given as

$$\Psi_{\text{iso}} = \frac{3}{2}\sum_{i=1}^{n}\frac{A_i}{1+\alpha_i}\left[\frac{\bar{I}_1}{3}\right]^{1+\alpha_i} + \frac{3}{2}\sum_{j=1}^{n}\frac{B_j}{1+\beta_j}\left[\frac{\bar{I}_2}{3}\right]^{1+\beta_j}, \tag{75}$$

where the $4n$ material parameters are splitted into a group of non-negative shear moduli $\{A_i, B_j\}$ and a group of exponents $\{\alpha_i, \beta_j\}$ having no real physical interpretation. Studies in [43] concerning a reasonable choice of n reported that eight parameters pairs, i.e. $n = 4$, are sufficient to obtain an accurate reproduction of

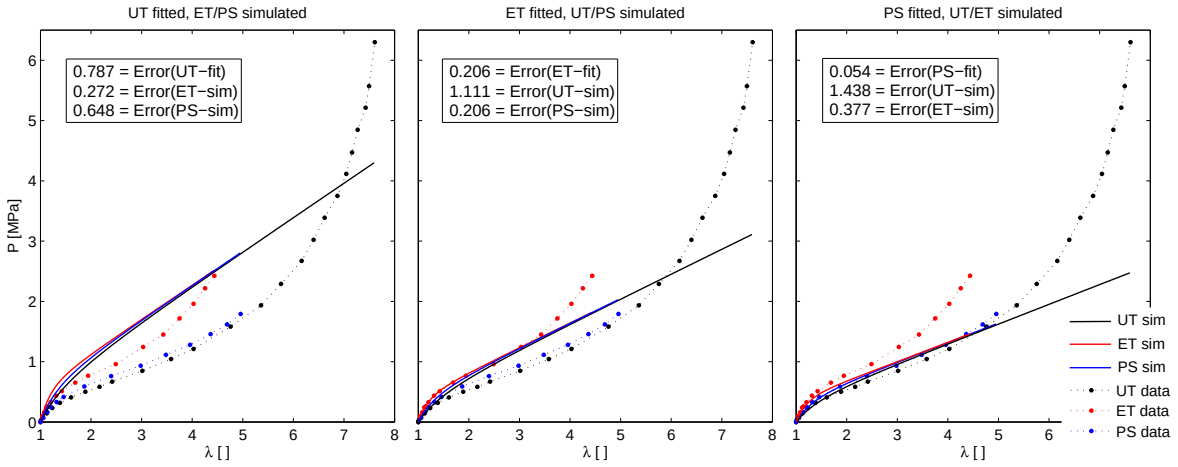

Fig. 8 Performance of the Gent and Thomas model on the Treloar data.

experiments, a result that has been approved on the Treloar data by Böl [56], who also stated a set of optimal parameters that is used here to confirm consistency of the tangent operator. From Eqns. (14) and (15) the fictitious stress tensor and the coefficients for the tangent operator follow as

$$\bar{\boldsymbol{S}} = \left[\sum_{i=1}^{n} A_i \left[\frac{\bar{I}_1}{3}\right]^{\alpha_i} + \bar{I}_1 \sum_{j=1}^{n} B_j \left[\frac{\bar{I}_2}{3}\right]^{\beta_j}\right] \boldsymbol{I} - \sum_{j=1}^{n} B_j \left[\frac{\bar{I}_2}{3}\right]^{\beta_j} \bar{\boldsymbol{C}} \tag{76}$$

$$\bar{\delta}_1 = \frac{2}{3}\sum_{i=1}^{n} A_i \alpha_i \left[\frac{\bar{I}_1}{3}\right]^{\alpha_i - 1} + 2\sum_{j=1}^{n} B_j \left[\frac{\bar{I}_2}{3}\right]^{\beta_j} + \frac{2}{3}\bar{I}_1^2 \sum_{j=1}^{n} B_j \beta_j \left[\frac{\bar{I}_2}{3}\right]^{\beta_j - 1} \tag{77}$$

$$\bar{\delta}_2 = -\frac{2}{3}\bar{I}_1 \sum_{j=1}^{n} B_j \beta_j \left[\frac{\bar{I}_2}{3}\right]^{\beta_j - 1} \quad , \quad \bar{\delta}_3 = \frac{2}{3}\sum_{j=1}^{n} B_j \beta_j \left[\frac{\bar{I}_2}{3}\right]^{\beta_j - 1} \quad , \quad \bar{\delta}_4 = -2\sum_{j=1}^{n} B_j \left[\frac{\bar{I}_2}{3}\right]^{\beta_j} . \tag{78}$$

For Böl's set of optimal Treloar parameters [56]

$$\boldsymbol{A} = [0.02672, 0.3594, -0.11075, 0.01074] \text{ MPa} \quad , \quad \boldsymbol{\alpha} = [-0.3, 0.2, 0.7, 1.5]$$
$$\boldsymbol{B} = [0.07522, -0.03588, 0.00576, -0.0001704] \text{ MPa} \quad , \quad \boldsymbol{\beta} = [-0.15, 0.1, 0.35, 0.75],$$

the local test converges quadratically to $\boldsymbol{C}_\infty = [1.57, 2.44, 1.23, 1.51, 0.0, 0.0]$:

Iteration n	0	1	2	3
$\|\boldsymbol{R}(\boldsymbol{C}_n)\|_2$	4.63e-01	1.31e-01	9.71e-04	4.39e-08
$\|\boldsymbol{C}_{n+1} - \boldsymbol{C}_n\|_2$	1.46e-01	1.73e-02	9.39e-05	9.48e-09

As before, the analytical $P_i(\lambda_i)$-relations for UT, ET and PS follow from Eqns. (20), (23), (26), whereas $\bar{I}_{1/2}^{UT/ET/PS}$ according to Eqns. (18), (21), (24) have to be inserted:

$$P_1^{UT} = \left[\sum_{i=1}^{n} A_i \left[\frac{\bar{I}_1^{UT}}{3}\right]^{\alpha_i} + \sum_{j=1}^{n} \frac{B_j}{\lambda}\left[\frac{\bar{I}_2^{UT}}{3}\right]^{\beta_j}\right]\left[\lambda - \frac{1}{\lambda^2}\right] \tag{79}$$

$$P_{1,2}^{ET} = \left[\sum_{i=1}^{n} A_i \left[\frac{\bar{I}_1^{ET}}{3}\right]^{\alpha_i} + \sum_{j=1}^{n} \lambda^2 B_j \left[\frac{\bar{I}_2^{ET}}{3}\right]^{\beta_j}\right]\left[\lambda - \frac{1}{\lambda^5}\right] \tag{80}$$

$$P_1^{PS} = \left[\sum_{i=1}^{n} A_i \left[\frac{\bar{I}^{PS}}{3}\right]^{\alpha_i} + \sum_{j=1}^{n} B_j \left[\frac{\bar{I}^{PS}}{3}\right]^{\beta_j}\right]\left[\lambda - \frac{1}{\lambda^3}\right] . \tag{81}$$

To evaluate performance and validity of Swanson's model we restrict ourselves to the cases $n = 1, 2$, which is mainly because a total number of twelve or sixteen parameters – the latter been proven to perfectly capture Treloar's data – cannot be considered to be manageable or efficient. Fitting each stress-stretch relation to the corresponding data provides the following sets of optimal material parameters:

$n=1$	$A_1^{UT} = 4.287\text{e-}5$ $B_1^{UT} = 0.4159$ $\alpha_1^{UT} = 3.128$ $\beta_1^{UT} = 1.085$	$A_1^{ET} = 0.4209$ $B_1^{ET} = 1.270\text{e-}3$ $\alpha_1^{ET} = -0.0936$ $\beta_1^{ET} = 0.4447$	$A_1^{PS} = 4.549\text{e-}3$ $B_1^{PS} = 0.3702$ $\alpha_1^{PS} = 1.529$ $\beta_1^{PS} = -0.202$
$n=2$	$\boldsymbol{A}^{UT} = [2.831\text{e-}3, 2.82\text{e-}13]$ $\boldsymbol{B}^{UT} = [1.871\text{e-}13, 0.4643]$ $\boldsymbol{\alpha}^{UT} = [1.684, 9.141]$ $\boldsymbol{\beta}^{UT} = [-0.4302, 0.7882]$	$\boldsymbol{A}^{ET} = [0.2101, 0.0074]$ $\boldsymbol{B}^{ET} = [0.1036, 0.2661]$ $\boldsymbol{\alpha}^{ET} = [-1833, 1.429]$ $\boldsymbol{\beta}^{ET} = [-6.634, -0.6232]$	$\boldsymbol{A}^{PS} = [0.0676, 3.266\text{e-}11]$ $\boldsymbol{B}^{PS} = [0.2861, 0.0267]$ $\boldsymbol{\alpha}^{PS} = [0.2687, 9.131]$ $\boldsymbol{\beta}^{PS} = [-0.4683, 0.7157]$

Figures 9 and 10 show the corresponding fits and simulations. Swanson's model precisely captures the experimental data, already in the simplest $n = 1$ version with only four parameters. Increasing to $n = 2$ (eight parameters) provides no further improvement in fitting quality, but requires much higher optimisation efforts. Parameters identified from UT overestimate the responses of the other modes by far and are not suited to gauge the model. This is not the case for parameters obtained from ET which yield again the best validation results. It is noteworthy that optimal A_2 parameters for UT and PS are very close to zero, i.e. higher-order $\bar{I}_1$-terms are obviously not activated by these deformation modes. This behaviour indicates different upper limits $m \neq n$ for the two sums in Eq. (75) to be reasonable.

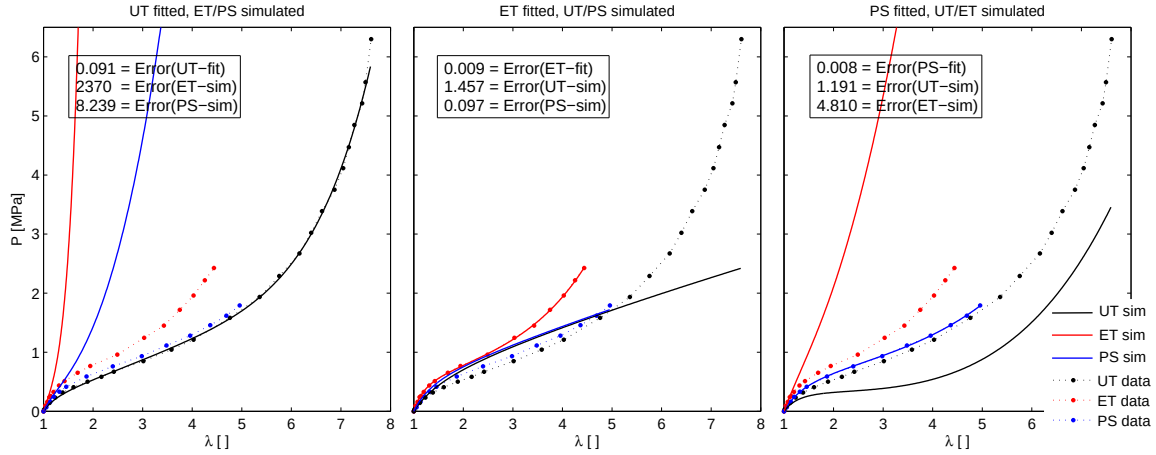

Fig. 9 Performance of the $(n = 1)$-Swanson model. Fit quality is perfect in all deformation modes, errors for ET and PS are negligible. Optimal UT parameters cannot reproduce other modes **(left)**, as is the case for ET **(middle)** and PS **(right)**. Merely simulating PS with ET parameters can be considered successful.

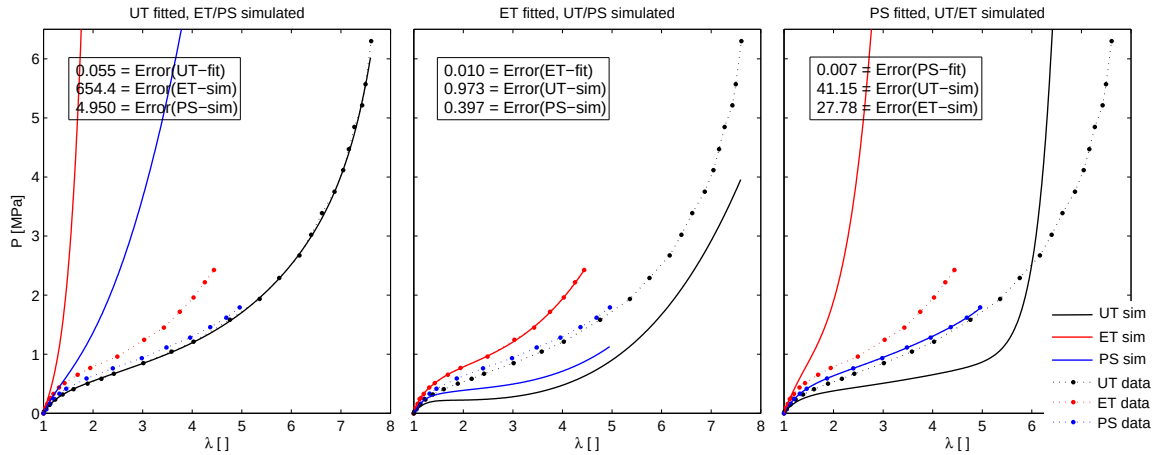

Fig. 10 Performance of the $(n = 2)$-Swanson model. To double the number of parameters hardly influences fit quality and validity (compare plots/errors of Fig. 9). In case of optimal ET parameters some qualitative improvement is observed, i.e. UT and PS simulations at least have the shape of the experimental curves now.

3.3.6 Yeoh model (1990)

Motivated by the experimental observation that the load-deformation curves of filled elastomers exhibit almost zero values $\partial\Psi/\partial\bar{I}_2 \approx 0$, Yeoh [45],[15] proposed an accordingly adapted function belonging to the class of Mooney-Rivlin models (38). It abstains from considering the second invariant in the free energy and includes all uncoupled $\bar{I}_1$ terms up to the power of three. Consequently, the isochoric free energy density reads

$$\Psi_{\text{iso}} = c_1 \left[\bar{I}_1 - 3\right] + c_2 \left[\bar{I}_1 - 3\right]^2 + c_3 \left[\bar{I}_1 - 3\right]^3, \tag{82}$$

where c_1, c_2, c_3 denote material parameters of shear modulus type and the second index for the neglected $\bar{I}_2$ terms is omitted. The typical nonlinear increase of the shear modulus at high strains is reproduced sufficiently accurate by this model due to the third-order $\bar{I}_1$ terms. A very similar model additionally incorporating the first $\bar{I}_2$ term has been proposed in 1958 by Biderman [46]. From Eqns. (14) and (15) fictitious stress tensor and tangent operator are computed to

$$\bar{\boldsymbol{S}} = \left[2c_1 + 4c_2 \left[\bar{I}_1 - 3\right] + 6c_3 \left[\bar{I}_1 - 3\right]^2\right] \boldsymbol{I} \tag{83}$$

$$\bar{\mathbb{C}} = J^{-\frac{4}{3}} \left[8c_2 + 24c_3 \left[\bar{I}_1 - 3\right]\right] \boldsymbol{I} \otimes \boldsymbol{I}. \tag{84}$$

For $[c_1, c_2, c_3] =$ [0.1634,-1.198e-3,3.781e-5], the local test (Appendix B) converges quadratically to $\boldsymbol{C}_\infty = [1.57, 2.44, 1.23, 1.51, 0.0, 0.0]$, as is indicated by the evolutions of residuals and strain updates:

Iteration n	0	1	2	3	4
$\|\boldsymbol{R}(\boldsymbol{C}_n)\|_2$	4.01e-01	1.44e-01	1.23e-03	7.46e-08	3.11e-15
$\|\boldsymbol{C}_{n+1} - \boldsymbol{C}_n\|_2$	1.44e-01	2.24e-02	1.34e-04	1.86e-08	1.52e-15

The analytical $P_i(\lambda_i)$-relations for UT, ET and PS are obtained from (20), (23), (26) as:

$$P_1^{UT} = \left[2c_1 + 4c_2 \left[\bar{I}_1^{UT} - 3\right] + 6c_3 \left[\bar{I}_1^{UT} - 3\right]^2\right] \left[\lambda - \lambda^{-2}\right] \tag{85}$$

$$P_{1,2}^{ET} = \left[2c_1 + 4c_2 \left[\bar{I}_1^{ET} - 3\right] + 6c_3 \left[\bar{I}_1^{ET} - 3\right]^2\right] \left[\lambda - \lambda^{-5}\right] \tag{86}$$

$$P_1^{PS} = \left[2c_1 + 4c_2 \left[\bar{I}_1^{PS} - 3\right] + 6c_3 \left[\bar{I}_1^{PS} - 3\right]^2\right] \left[\lambda - \lambda^{-3}\right]. \tag{87}$$

The optimal parameter sets after fitting each equation to the corresponding Treloar data are:

$$\left[c_1^{UT}, c_2^{UT}, c_3^{UT}\right] = [0.1634,-1.198e-3,3.781e-5] \tag{88}$$

$$\left[c_1^{ET}, c_2^{ET}, c_3^{ET}\right] = [0.2059,-7.124e-4,3.078e-5] \tag{89}$$

$$\left[c_1^{PS}, c_2^{PS}, c_3^{PS}\right] = [0.1776,-1.620e-3,5.033e-5]. \tag{90}$$

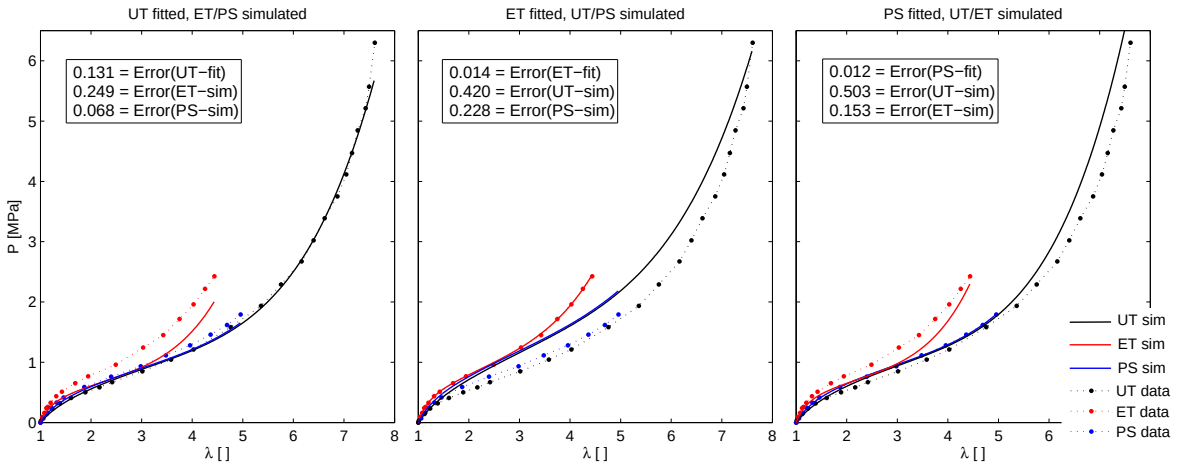

Fig. 11 Performance of Yeoh's model on the Treloar data. The fitting quality is good to excellent, especially in consideration of the low number of parameters. Uniaxial and pure shear parameters are fairly coincident, **(left)** vs. **(right)**, both numerically and in underestimating equibiaxial data. ET-fitted parameters systematically overestimate UT and PS.

Concerning the validity of the model, each parameter set is used to simulate the other two deformation modes. The results are plotted in Fig. 11, together with fitting and simulation errors. The cubic character of Yeoh's model is obviously suited to reproduce the S-shape at large strains. Nonetheless, a comparison of the UT-fitting errors with those of Swanson's models reveals that the restriction to integer exponents of $\bar{I}_1$ may not be the ideal choice to approximate arbitrary changes in curvature. On the other hand, as indicated by the almost perfect approximation of the ET- and PS-data, this may also depend on the range of stretches used for parameter optimisation. Furthermore, it can be stated that each set of optimal parameters yields simulation results for the complementary deformation modes that are quantitatively much more reasonable than for any other of the previous models. This is particularly remarkable since $\bar{I}_2$ is missing in Ψ_{iso} and the small number of only three material parameters.

3.3.7 Arruda-Boyce model (1993) (invariant form)

Arruda and Boyce [6] developed a highly regarded constitutive model for rubber-like materials by assuming that the macromolecular polymer network can locally be represented by eight chains that are oriented from the center along the diagonals of a cube. The edges of this cube are thereby aligned with the eigendirections of $\bar{\boldsymbol{C}}$ and stretched by the corresponding eigenvalues. The resulting chain deformations lead to forces according to an energy function that is governed by the inverse Langevin function, i.e. by non-Gaussian statistics, cf. also Section 4. Since there is no analytical inversion of Langevin's function available, various different types of approximation have been applied providing different formats of the corresponding free energy density Ψ_{iso}. In section 4.2 the micromechanical version usually referred to as *eight chain model* will be discussed, which makes use of a Padé approximation to substitute the inverse Langevin function. Another approach considers a series expansion leading to the following convenient, invariant-based energy formulation

$$\Psi_{\text{iso}} = \mu \sum_{k=1}^{K} \frac{C_k}{N^{k-1}} \left[\bar{I}_1^k - 3^k\right] , \tag{91}$$

in which μ is denoting the shear modulus, N is the number of Kuhn [57] segments per polymer chain and the first five coefficients C_k are

$$[C_1, C_2, C_3, C_4, C_5] = \left[\frac{1}{2}, \frac{1}{20}, \frac{11}{1050}, \frac{19}{7000}, \frac{519}{673750}\right] . \tag{92}$$

Since only $\bar{I}_1$ is contained in free energy density (91), the evaluation of Eqns. (14) and (15) is inexpensive and yields the following results for fictitious stress tensor and tangent operator:

$$\bar{\boldsymbol{S}} = \left[2\mu \sum_{k=1}^{K} \frac{k\, C_k}{N^{k-1}}\, \bar{I}_1^{k-1}\right] \boldsymbol{I} \tag{93}$$

$$\bar{\mathbb{C}} = \left[4J^{-\frac{4}{3}}\mu \sum_{k=1}^{K} \frac{[k^2-k]\, C_k}{N^{k-1}}\, \bar{I}_1^{k-2}\right] \boldsymbol{I} \otimes \boldsymbol{I}. \tag{94}$$

With parameters chosen as $[\mu, N] = [0.2424 \text{ MPa}, 20.25]$, the local test (Appendix B) converges quadratically to $\boldsymbol{C}_\infty = [1.56, 2.43, 1.22, 1.51, 0.0, 0.0]$, cf. the evolutions of residuals and strain updates:

Iteration n	0	1	2	3
$\|\boldsymbol{R}(\boldsymbol{C}_n)\|_2$	4.74e-01	1.21e-01	8.76e-04	3.16e-08
$\|\boldsymbol{C}_{n+1} - \boldsymbol{C}_n\|_2$	1.39e-01	1.83e-02	9.42e-05	9.78e-09

The analytical $P_i(\lambda_i)$-relations follow from (20), (23), (26) with $\bar{I}_1^{UT/ET/PS}$ as in (18), (21), (24):

$$P_1^{UT} = \left[\sum_{k=1}^{K} \frac{2\mu^{UT} k\, C_k}{[N^{UT}]^{k-1}} [\bar{I}_1^{UT}]^{k-1}\right] \left[\lambda - \lambda^{-2}\right] \tag{95}$$

$$P_{1,2}^{ET} = \left[\sum_{k=1}^{K} \frac{2\mu^{ET} k\, C_k}{[N^{ET}]^{k-1}} [\bar{I}_1^{ET}]^{k-1}\right] \left[\lambda - \lambda^{-5}\right] \tag{96}$$

$$P_1^{PS} = \left[\sum_{k=1}^{K} \frac{2\mu^{PS} k\, C_k}{[N^{PS}]^{k-1}} [\bar{I}_1^{PS}]^{k-1}\right] \left[\lambda - \lambda^{-3}\right] . \tag{97}$$

Fitting each of these equations to the corresponding Treloar data yields the following material parameter sets:

$$\mu^{UT} = 0.2424\,\text{MPa} \quad , \quad \mu^{ET} = 0.3591\,\text{MPa} \quad , \quad \mu^{PS} = 0.3124\,\text{MPa} \tag{98}$$

$$N^{UT} = 20.25 \quad , \quad N^{ET} = 27.73 \quad , \quad N^{PS} = 50.33\,. \tag{99}$$

Figure 12 depicts the corresponding fits together with the simulations of the complementary deformation modes not used for parameter identification as well as the differences to Treloar's data. Although experimental findings are reproduced well, some improvement regarding the general validity of parameters would be desirable and can probably be realised by considering additional terms in the free energy. In view of the structural interpretation of N as number of Kuhn segments, i.e. chain length, it can hardly be considered admissible that three different values for N are obtained since not the tested material structure has been changed but only the deformation mode.

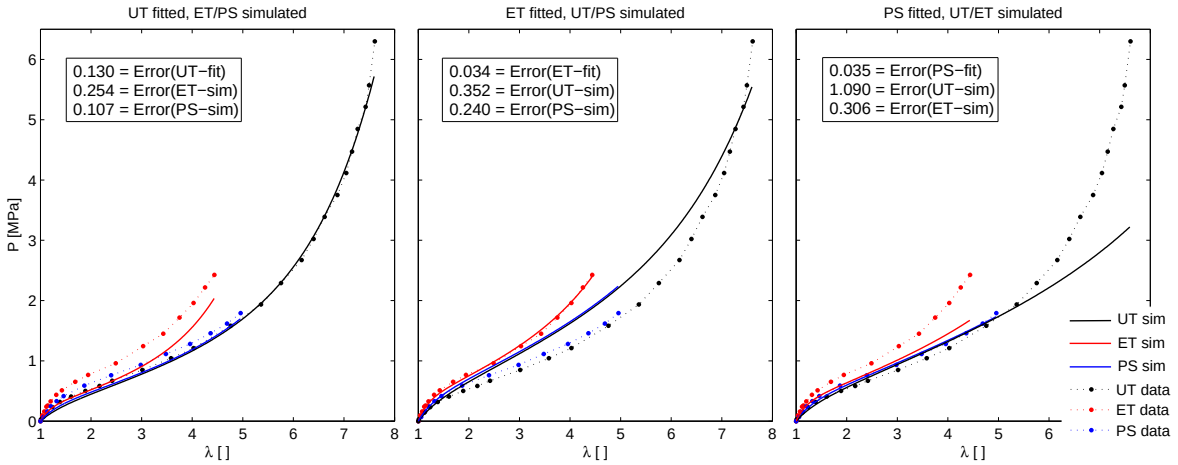

Fig. 12 Performance of Arruda-Boyce model on the Treloar data. The fitting quality is quite good, especially if compared to models having similarly few parameters, e.g. Neo-Hooke and Mooney-Rivlin. Identified parameters also have a more general validity in the sense that they qualitatively reproduce the other deformation modes, although over- and underestimations are not satisfying but follow the same trends observed already for the previous models.

3.3.8 Gent model (1996)

Another sophisticated, phenomenologically motivated two-parameter model has been proposed by Gent [29]. Horgan and Saccomandi [31], [32] have later derived a micromechanical re-interpretation and proved Gent's model to have some similarity to the inverse Langevin ansatz proposed already by James and Guth [47] and Treloar [54]. Especially finite chain extensibility is accounted for by the parameter J_m which ensures the blow-up of the logarithmic energy function for limiting values of $[\bar{I}_1 - 3]$:

$$\Psi_{\text{iso}} = -J_m \, \frac{\mu}{2} \, \ln\left(1 - \frac{\bar{I}_1 - 3}{J_m}\right) . \tag{100}$$

Again, μ is a shear modulus type material parameter. Fictitious stress tensor and tangent operator follow as

$$\bar{\boldsymbol{S}} = \left[\frac{\mu J_m}{J_m - \bar{I}_1 + 3}\right] \boldsymbol{I} \tag{101}$$

$$\bar{\mathbb{C}} = J^{-\frac{4}{3}} \left[\frac{2\mu J_m}{[J_m - \bar{I}_1 + 3]^2}\right] \boldsymbol{I} \otimes \boldsymbol{I}. \tag{102}$$

from evaluation of Eqns. (14) and (15). With parameters chosen as $[\mu, J_m] = [0.2514\,\text{MPa}, 81.16]$, the local test (Appendix B) converges quadratically to $\boldsymbol{C}_\infty = [1.87, 3.02, 1.14, 1.99, 0.0, 0.0]$:

Iteration n	0	1	2	3
$\|\boldsymbol{R}(\boldsymbol{C}_n)\|_2$	5.54e-01	1.20e-01	6.93e-04	3.18e-08
$\|\boldsymbol{C}_{n+1} - \boldsymbol{C}_n\|_2$	1.81e-01	1.40e-02	5.29e-05	5.21e-09

The analytical $P_i(\lambda_i)$-relations follow from (20), (23), (26) with $\bar{I}_1^{UT/ET/PS}$ inserted from (18), (21), (24):

$$P_1^{UT} = \frac{\mu^{UT} J_m^{UT} \left[\lambda^3 - 1\right]}{\lambda \left[\lambda J_m^{UT} - \lambda^3 + 3\lambda - 2\right]} \tag{103}$$

$$P_{1,2}^{ET} = \frac{\mu^{ET} J_m^{ET} \left[\lambda^6 - 1\right]}{\lambda \left[\lambda^4 J_m^{ET} - 2\lambda^6 + 3\lambda^4 - 1\right]} \tag{104}$$

$$P_1^{PS} = \frac{\mu^{PS} J_m^{PS} \left[\lambda^4 - 1\right]}{\lambda \left[\lambda^2 J_m^{PS} - \lambda^4 + 2\lambda^2 - 1\right]}. \tag{105}$$

Fitting each of these equations to the corresponding Treloar data yields the following material parameter sets:

$$\mu^{UT} = 0.2514 \text{ MPa} \quad , \quad \mu^{ET} = 0.3630 \text{ MPa} \quad , \quad \mu^{PS} = 0.3166 \text{ MPa} \tag{106}$$

$$J_m^{UT} = 81.16 \quad , \quad J_m^{ET} = 111.9 \quad , \quad J_m^{PS} = 237.7\,. \tag{107}$$

Figure 13 shows the fitted curves, the simulations of complementary deformation modes not used for parameter optimisation and the errors wrt to Treloar's data. The capability of the model to reproduce the experimental data as well as the validity of the material constants are – even numerically – very close to those obtained for Arruda-Boyce' and Yeoh's models.

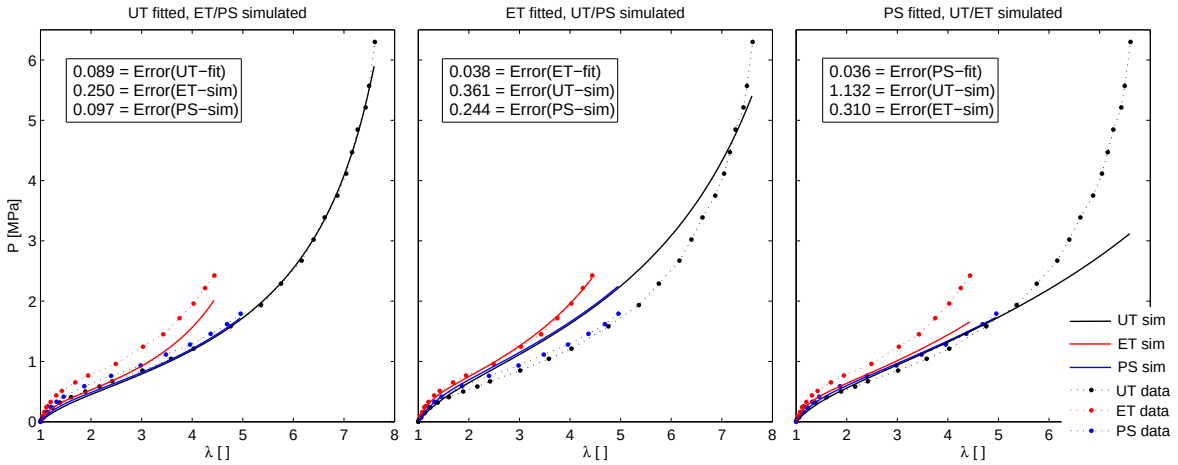

Fig. 13 Performance of Gent's model on the Treloar data. Fitting quality and validity of the parameters are very similar to those of the Arruda-Boyce and Yeoh models.

3.3.9 Yeoh-Fleming model (1997)

The model by Yeoh and Fleming [16] links concepts from statistical mechanics and phenomenological approaches to rubber elasticity. It adapts features from the ansatzes proposed earlier by Gent [29] and Yeoh [15], namely a logarithmic term ensuring energy blow-up for chains reaching their maximum stretch and another exponential part capturing the nonlinearities at small strains. As its predecessors the model does not consider influences of the second invariant $\bar{I}_2$. The isochoric free energy density according to [16]

$$\Psi_{\text{iso}} = \frac{A}{B}\left[1 - \exp\left(-B[\bar{I}_1 - 3]\right)\right] - C[I_m - 3]\ln\left(1 - \frac{\bar{I}_1 - 3}{I_m - 3}\right) \tag{108}$$

is governed by the four material parameters A, B, C, I_m. Fictitious stress tensor and tangent operator follow from evaluating Eqns. (14) and (15):

$$\bar{\boldsymbol{S}} = \left[2A\exp\left(-B[\bar{I}_1 - 3]\right) + 2C\frac{I_m - 3}{I_m - \bar{I}_1}\right]\boldsymbol{I} \tag{109}$$

$$\bar{\mathbb{C}} = 4J^{-\frac{4}{3}}\left[-AB\exp\left(-B[\bar{I}_1 - 3]\right) + C\frac{I_m - 3}{[I_m - \bar{I}_1]^2}\right]\boldsymbol{I}\otimes\boldsymbol{I}. \tag{110}$$

With parameters chosen as $[A, B, C, I_m] = [0.0517, 0.2362, 0.1235, 83.23]$, the local test (Appendix B) converges quadratically to $\boldsymbol{C}_\infty = [1.57, 2.44, 1.23, 1.51, 0.0, 0.0]$:

Iteration n	0	1	2	3
$\|\boldsymbol{R}(\boldsymbol{C}_n)\|_2$	4.75e-01	1.21e-01	8.72e-04	3.14e-08
$\|\boldsymbol{C}_{n+1} - \boldsymbol{C}_n\|_2$	1.47e-01	1.64e-02	7.63e-05	7.14e-09

The analytical $P_i(\lambda)$-relations follow from (20), (23), (26) with $\bar{I}_1^{UT/ET/PS}$ inserted from (18), (21), (24):

$$P_1^{UT} = \frac{2A^{UT}[\lambda^3 - 1]}{\lambda^2} \exp\left(-B^{UT}\frac{\lambda^3 - 3\lambda + 2}{\lambda}\right) + \frac{2C^{UT}[I_m^{UT} - 3][\lambda^3 - 1]}{I_m^{UT}\lambda^2 - \lambda^4 - 2\lambda} \tag{111}$$

$$P_{1,2}^{ET} = \frac{2A^{ET}[\lambda^6 - 1]}{\lambda^5} \exp\left(-B^{ET}\frac{2\lambda^6 - 3\lambda^4 + 1}{\lambda^4}\right) + \frac{2C^{ET}[I_m^{ET} - 3][\lambda^6 - 1]}{I_m^{ET}\lambda^5 - 2\lambda^7 - \lambda} \tag{112}$$

$$P_1^{PS} = \frac{2A^{PS}[\lambda^4 - 1]}{\lambda^3} \exp\left(-B^{PS}\frac{\lambda^4 - 2\lambda^2 + 1}{\lambda^2}\right) + \frac{2C^{PS}[I_m^{PS} - 3][\lambda^4 - 1]}{I_m^{PS}\lambda^3 - \lambda^5 - \lambda^3 - \lambda}. \tag{113}$$

Fitting each of these equations to the corresponding Treloar data yields the following material parameter sets:

$$\left[A^{UT}, B^{UT}, C^{UT}, I_m^{UT}\right] = [0.0517, 0.2362, 0.1235, 83.23] \tag{114}$$

$$\left[A^{ET}, B^{ET}, C^{ET}, I_m^{ET}\right] = [0.0467, 0.1303, 0.1635, 93.35] \tag{115}$$

$$\left[A^{PS}, B^{PS}, C^{PS}, I_m^{PS}\right] = [0.0512, 0.1976, 0.1350, 94.13]\,. \tag{116}$$

As a consequence of the model's extreme nonlinearity together with its significant four-parameter flexibility the optimisation procedure becomes highly sensitive to the choice of initial values. Figure 14 depicts the fitting results, the simulations of complementary deformation modes not used for parameter optimisation and the errors wrt Treloar's data.

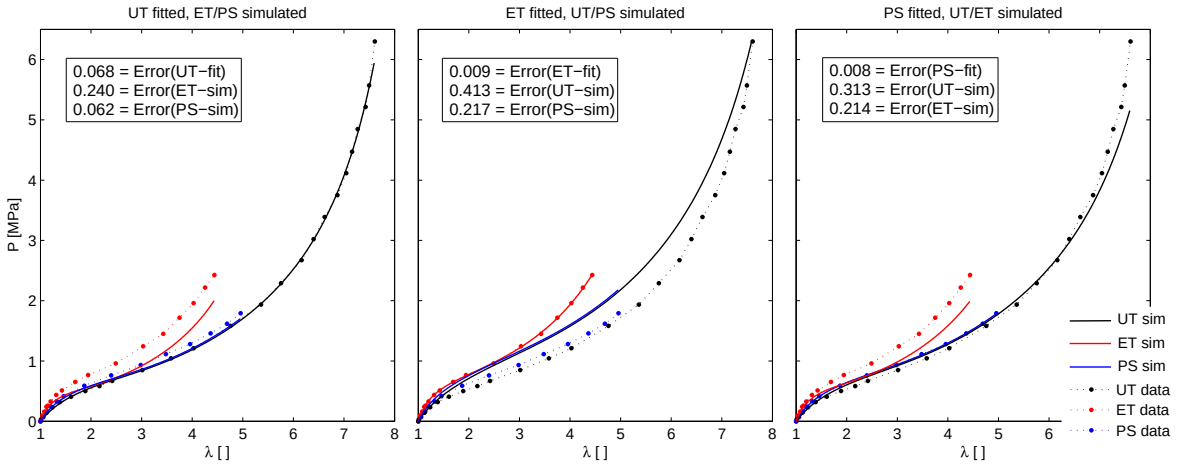

Fig. 14 Performance of the Yeoh-Fleming model on the Treloar data. Reproduction of experiments is consistently perfect, the general validity of parameters is lacking some quantitative accuracy, i.e. the previously observed over- and underestimations occur, although all simulations very well capture the shapes of the curves.

3.3.10 Carroll model (2011)

Carroll [62] proposed another phenomenological approach. Its isochoric free energy density

$$\Psi_{\text{iso}} = a\bar{I}_1 + b\bar{I}_1^4 + c\sqrt{\bar{I}_2} \tag{117}$$

is governed by three material parameters a, b, c. Fictitious stress tensor (14) and the coefficients $\bar{\delta}_{1\ldots4}$ required for tangent operator (15) follow as:

$$\bar{\boldsymbol{S}} = \left[2a + 8b\bar{I}_1^3\right]\boldsymbol{I} + \frac{c}{\sqrt{\bar{I}_2}}[\bar{I}_1\boldsymbol{I} - \bar{\boldsymbol{C}}] \tag{118}$$

$$\bar{\delta}_1 = 48b\bar{I}_1 + \frac{c[2 - \bar{I}_2]}{4\sqrt{\bar{I}_2}} \quad , \quad \bar{\delta}_2 = c\bar{I}_1\bar{I}_2^{-3/2} \quad , \quad \delta_3 = -c\bar{I}_2^{-3/2} \quad , \quad \delta_4 = -\frac{2c}{\sqrt{\bar{I}_2}}. \tag{119}$$

With parameters chosen as $[a, b, c] = [0.1481, 3.024\text{e-}7, 0.06623]$, the local tangent test quadratically converges to $\boldsymbol{C}_\infty = [1.57, 2.44, 1.23, 1.51, 0.0, 0.0]$:

Iteration n	0	1	2	3
$\|\boldsymbol{R}(\boldsymbol{C}_n)\|_2$	4.75e-01	1.21e-01	8.72e-04	3.14e-08
$\|\boldsymbol{C}_{n+1} - \boldsymbol{C}_n\|_2$	1.47e-01	1.64e-02	7.63e-05	7.14e-09

The analytical $P_i(\lambda)$-relations follow from (20), (23), (26) with $\bar{I}_1^{UT/ET/PS}$ inserted from (18), (21), (24):

$$P_1^{UT} = \left[2a + 8b\left[2\lambda^{-1} + \lambda^2\right]^3 + c\left[1 + 2\lambda^3\right]^{-1/2}\right]\left[\lambda - \lambda^{-2}\right] \tag{120}$$

$$P_{1,2}^{ET} = \left[2a + 8b\left[\lambda^{-4} + 2\lambda^2\right]^3 + c\left[2\lambda^2 + \lambda^8\right]^{-1/2}\right]\left[\lambda - \lambda^{-5}\right] \tag{121}$$

$$P_1^{PS} = \left[2a + 8b\left[\lambda^2 + \lambda^{-2} + 1\right]^3 + c\left[\lambda^2 + \lambda^{-2} + 1\right]^{-1/2}\right]\left[\lambda - \lambda^{-3}\right]\,. \tag{122}$$

Fitting each of these equations to the corresponding Treloar data yields the following material parameter sets:

$$\left[a^{UT}, b^{UT}, c^{UT}\right] = [0.1481, 3.024\text{e-}7, 0.06623]\ \text{MPa} \tag{123}$$

$$\left[a^{ET}, b^{ET}, c^{ET}\right] = [0.1957, 3.445\text{e-}7, 0.06983]\ \text{MPa} \tag{124}$$

$$\left[a^{PS}, b^{PS}, c^{PS}\right] = [0.1297, 4.910\text{e-}7, 0.18760]\ \text{MPa}\,. \tag{125}$$

As a consequence of the model's extreme nonlinearity together with its significant four-parameter flexibility the optimisation procedure becomes highly sensitive to the choice of initial values. Figure 15 depicts the fitting results, the simulations of complementary deformation modes not used for parameter optimisation and the errors wrt Treloar's data.

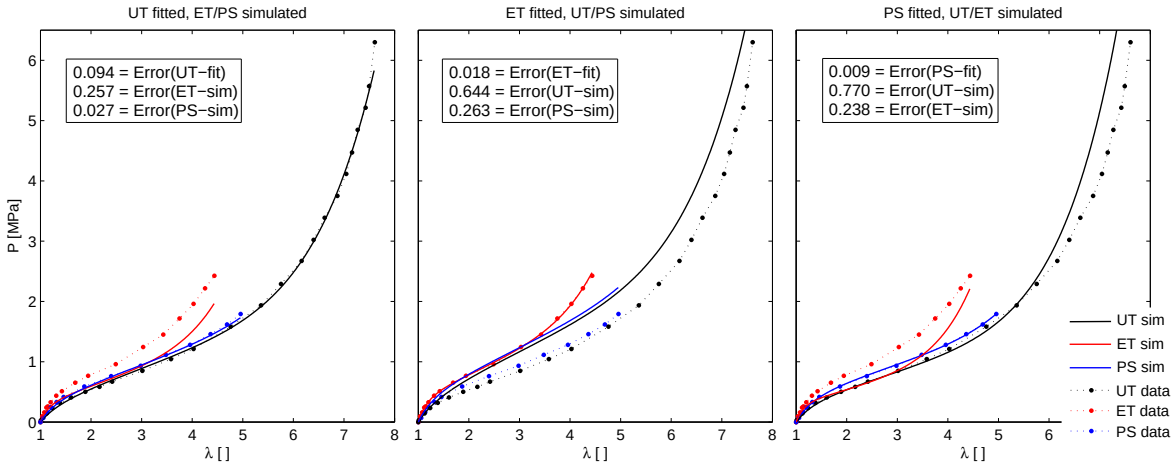

Fig. 15 Performance of the Carroll model on the Treloar data.

4 Micro-mechanical models: Stress tensors, tangent operators and performance

Micro-mechanical approaches to rubber elasticity usually depart from a description of the deformation behaviour of a single polymer chain. The macro-molecule constituting the chain is itself build from a certain number of chemically identical repeat units, the so-called monomers. This structure is modelled as a chain of N freely jointed, rigid beams of length l which are allowed to be arbitrarily oriented with respect to each other. The beams are frequently denoted as *Kuhn segments* and the assumption of free rotation usually requires that each segment comprises multiple monomers since real bond angles only can take certain admissible values. The maximum distance between the two chain ends equals its contour length $r_{\max} = Nl$, i.e. if the

chain is fully elongated and all segments are aligned identically. From statistical considerations (*random walk chain*) the end-to-end distance of a stress-free undeformed chain results as $r_0 = \sqrt{N}l$, which motivates the introduction of the following *chain stretch*:

$$\lambda = \frac{r}{r_0} = \frac{r}{\sqrt{N}l} \in [0, \sqrt{N}]\,. \tag{126}$$

Similar to macroscopic continua, the elastic behaviour of a single chain is described in terms of a scalar free energy function, which will here be denoted by $\psi = \psi(\lambda)$. Two prominent examples are the so-called Gauss and Langevin chains, respectively, whose energy functions are given by

$$\psi^{\text{Gauss}}(\lambda) = \frac{3}{2} k_B \Theta \lambda^2 + \psi_0 \tag{127}$$

$$\psi^{\text{Langevin}}(\lambda) = k_B \Theta N \left[\frac{\lambda}{\sqrt{N}} \mathcal{L}^{-1}\left(\lambda\sqrt{N^{-1}}\right) + \ln\left(\frac{\mathcal{L}^{-1}\left(\lambda\sqrt{N^{-1}}\right)}{\sinh\left(\mathcal{L}^{-1}\left(\lambda\sqrt{N^{-1}}\right)\right)} \right) \right] + \psi_0 \tag{128}$$

and wherein k_B, Θ and $\mathcal{L}^{-1}$ denote Boltzmann's constant, absolute temperature and inverse of the Langevin function $\mathcal{L}(\bullet) = \coth(\bullet) - (\bullet)^{-1}$, respectively. Note that the Gaussian chain is valid only for moderate stretches $\lambda \ll \sqrt{N}$ since the corresponding chain force

$$f^{\text{Gauss}}(\lambda) = \frac{\partial \psi^{\text{Gauss}}}{\partial \lambda} = 3 k_B \Theta \lambda \tag{129}$$

is a linear function and does not adequately reflect finite chain extensibility, i.e. the dramatic force increase required if the chain approaches its maximal end-to-end distance $r_{\max}$. In numerical applications, the inverse of Langevin's function is usually substituted by the following Padé approximation:

$$\mathcal{L}^{-1}\left(\lambda\sqrt{N^{-1}}\right) \approx \lambda\sqrt{N^{-1}} \frac{3N - \lambda^2}{N - \lambda^2}\,. \tag{130}$$

With the above type of chain description macroscopic material models are derived by averaging the energies of a certain ensemble of chains, which ideally is chosen such that it reflects the mechanical behaviour of the true polymer network as realistic as possible:

$$\Psi_{\text{iso}} = \Psi_{\text{iso}}\big(\bar{\boldsymbol{C}}\big) := n \,\langle \psi \rangle \approx \frac{n}{K} \sum_{k=1}^{K} \psi(\lambda_k). \tag{131}$$

We remain here with the assumption of incompressibility and the corresponding energy decomposition of the previous sections and consider purely isochoric behaviour. The number of chains K as well as their spatial orientations are decisive with regard to qualitative behaviour and (an)isotropy of the model, whereas the chain density n quantitatively relates micro- and macro stiffnesses. Furthermore, some relation between macroscopic deformation $\bar{\boldsymbol{C}}$ and chain stretches λ_k has to be defined, for which non-affine as well as affine approaches like the following have been proposed in the literature: If we assume the initially unstretched chain to be aligned with a unit normal vector $\boldsymbol{t}_k^0$, its end-to-end vector reads $\boldsymbol{r}_k^0 = \sqrt{N}l\boldsymbol{t}_k^0$ and a deformation gradient $\bar{\boldsymbol{F}}$ implies $\boldsymbol{r}_k = \bar{\boldsymbol{F}}\boldsymbol{r}_k^0$ for the end-to-end vector of the correspondingly stretched chain. Consequently,

$$\lambda_k = \frac{\|\boldsymbol{r}_k\|}{\|\boldsymbol{r}_k^0\|} = \frac{\sqrt{<\bar{\boldsymbol{F}}\boldsymbol{r}_k^0, \bar{\boldsymbol{F}}\boldsymbol{r}_k^0>}}{\sqrt{N}l} = \frac{\sqrt{N}l\sqrt{<\boldsymbol{t}_k^0, \bar{\boldsymbol{F}}^T\bar{\boldsymbol{F}}\boldsymbol{t}_k^0>}}{\sqrt{N}l} = \sqrt{<\boldsymbol{t}_k^0, \bar{\boldsymbol{C}}t_k^0>} = \sqrt{\bar{\boldsymbol{C}} : [\boldsymbol{t}_k^0 \otimes \boldsymbol{t}_k^0]} \tag{132}$$

as required to evaluate Eq. (131). Three different micro-mechanical models as resulting from certain choices of chain energy ψ, chain number K, initial chain orientations $\boldsymbol{t}_k^0$ and micro-macro stretch relations $\lambda_k = \lambda_k\big(\bar{\boldsymbol{C}}\big)$ will be discussed in the following subsections.
For macroscopic energy densities defined as in Eq. (131), the corresponding isochoric stress tensors and tangent operators required for finite element implementation can again be calculated from Eq. (5) together with $\bar{\boldsymbol{S}} = 2\partial\Psi_{\text{iso}}(\bar{\boldsymbol{C}})/\partial\bar{\boldsymbol{C}}$ and Eq. (7), respectively.

Regarding the analytical stress-stretch relations for UT, ET and PS, which are essential to evaluate the performance of also the micro-mechanical models on Treloar's data, we consider a re-parametrisation of $\Psi_{\rm iso}$ in terms of the isochoric principal macro stretches λ_i. From Eq. (16), the pressure p follows as

$$p = \lambda_j \frac{\partial \Psi_{\rm iso}}{\partial \lambda_j} \tag{133}$$

from a nominal principal stress P_j being zero due to the type of deformation, e.g. $P_2 = 0$ in case of uniaxial tension. Re-inserted into (16), utilisation of chain energy average (131) yields

$$\begin{aligned} P_i &= \frac{\partial \Psi_{\rm iso}}{\partial \lambda_i} - \frac{\lambda_j}{\lambda_i}\frac{\partial \Psi_{\rm iso}}{\partial \lambda_j} \quad , \quad i \in \{1,2,3\} \ , \ j \text{ such that } P_j = 0 \\ &= \frac{n}{K}\sum_{k=1}^{K} \frac{\partial \psi}{\partial \Lambda_k}\frac{\partial \Lambda_k}{\partial \lambda_i} - \frac{n}{K}\frac{\lambda_j}{\lambda_i}\sum_{k=1}^{K} \frac{\partial \psi}{\partial \Lambda_k}\frac{\partial \Lambda_k}{\partial \lambda_j} \, . \end{aligned} \tag{134}$$

Therein, the derivatives of chain stretches Λ_k wrt principal macro stretches λ_i follow from corresponding relations like (132) while the chain forces $f_k = \partial\psi(\Lambda_k)/\partial\Lambda_k$ are given by (129) for the Gaussian case and

$$\frac{\partial \psi^{\rm Langevin}}{\partial \Lambda_k} = k_B \Theta \sqrt{N} \mathcal{L}^{-1}\left(\Lambda_k \sqrt{N^{-1}}\right) , \tag{135}$$

for the Langevin chain, respectively, compare e.g. [9].

4.1 Three chain model (1943)

The three chain model [47],[48] locally substitutes the true polymer network by $K = 3$ chains and assumes each of them to be aligned with one of the principal directions $\boldsymbol{N}_i$ of the isochoric right Cauch-Green tensor, cf. Figure 16. As before, only the isochoric part of the deformation is considered and modelled, i.e. all overbars are again omitted for simplicity.

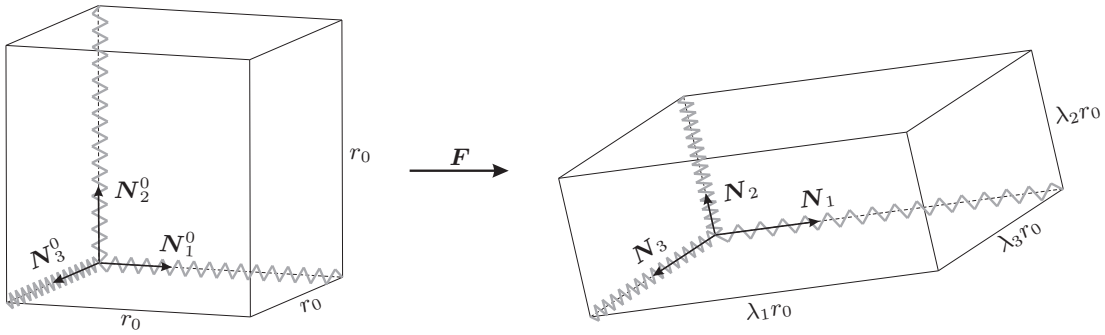

Fig. 16 Three chain model: initial and deformed chain orientations and stretches

It is obvious from the particular choice of their orientations, that the stretch of each chain is equal to the corresponding isochoric principal stretch, i.e.

$$\Lambda_k = \lambda_k \quad , \quad k = 1,2,3. \tag{136}$$

Regarding the free chain energy ψ, both the Gaussian and Langevin ansatzes have been discussed in the literature. While insertion of (127) with (136) into (131) yields a macroscopic model behaving identically to the Neo-Hookean, the incorporation of the more sophisticated Langevin chain provides a rubber model which is valid also at very large strains. Resorting to the frequently used definitions for shear modulus $\mu = nk_B\Theta$ and inverse Langevin function $\gamma_k = \mathcal{L}^{-1}(\sqrt{N^{-1}}\Lambda_k)$ the macroscopic free energy density is given as

$$\Psi_{\rm iso} = \frac{n}{3}\sum_{k=1}^{3} \psi^{\rm Langevin}(\Lambda_k) = \frac{\mu N}{3}\sum_{k=1}^{3}\left[\sqrt{N^{-1}}\lambda_k\gamma_k + \ln\left(\frac{\gamma_k}{\sinh(\gamma_k)}\right)\right] \tag{137}$$

according to Eq. (131) together with (136) in (128). The corresponding fictitious stress tensor $\bar{\boldsymbol{S}} = 2\partial\Psi_{\text{iso}}/\partial\bar{\boldsymbol{C}}$ then follows from the chain rule, Eq. (135) with Padé approximation (130) and in view of

$$\begin{aligned}\frac{\partial\Lambda_k}{\partial\bar{\boldsymbol{C}}} &\overset{(136)}{=} \frac{\partial\lambda_k}{\partial\bar{\boldsymbol{C}}} \overset{(132)}{=} \frac{\partial\sqrt{\bar{\boldsymbol{C}} : \left[\boldsymbol{N}_k^0 \otimes \boldsymbol{N}_k^0\right]}}{\partial\bar{\boldsymbol{C}}} \\ &= \frac{1}{2}\left[\bar{\boldsymbol{C}} : \left[\boldsymbol{N}_k^0 \otimes \boldsymbol{N}_k^0\right]\right]^{-\frac{1}{2}} \frac{\partial\bar{\boldsymbol{C}}}{\partial\bar{\boldsymbol{C}}} : \left[\boldsymbol{N}_k^0 \otimes \boldsymbol{N}_k^0\right] \\ &= \frac{1}{2}\lambda_k^{-1}\left[\boldsymbol{N}_k^0 \otimes \boldsymbol{N}_k^0\right] , \end{aligned} \tag{138}$$

respectively, and is only dependent on the isochoric principal stretches:

$$\bar{\boldsymbol{S}} = \frac{\mu}{3}\sum_{k=1}^{3}\frac{3N-\lambda_k^2}{N-\lambda_k^2}\left[\boldsymbol{N}_k^0 \otimes \boldsymbol{N}_k^0\right] . \tag{139}$$

Fictitious tangent operator $\bar{\mathbb{C}}$ requires another derivation wrt $\bar{\boldsymbol{C}}$ which provides the following equation

$$\bar{\mathbb{C}} = \frac{2}{3}\mu J^{-\frac{4}{3}}\sum_{k=1}^{3}\left[\frac{2N}{\left[N-\lambda_k^2\right]^2}\left[\boldsymbol{N}_k^0 \otimes \boldsymbol{N}_k^0 \otimes \boldsymbol{N}_k^0 \otimes \boldsymbol{N}_k^0\right] + \left[\frac{3N-\lambda_k^2}{N-\lambda_k^2}\right]\frac{\partial\left(\boldsymbol{N}_k^0 \otimes \boldsymbol{N}_k^0\right)}{\partial\bar{\boldsymbol{C}}}\right] . \tag{140}$$

Concerning details on the here required computation of $\partial\left(\boldsymbol{N}_k^0 \otimes \boldsymbol{N}_k^0\right)/\partial\bar{\boldsymbol{C}}$ the interested reader is referred to Appendix C. For material parameters chosen as $[\mu, N] = [0.2681\text{ MPa}, 77.29]$, the local convergence test introduced in Appendix B quadratically converges to $\boldsymbol{C}_\infty = [1.67, 2.64, 1.92, 1.68, 0.0, 0.0]$, as is indicated by the evolutions of the Euclidean norms of residuals and strain updates:

Iteration n	0	1	2	3
$\left\|\boldsymbol{R}(\boldsymbol{C}_n)\right\|_2$	5.21e-01	1.18e-01	7.56-04	3.27e-08
$\left\|\boldsymbol{C}_{n+1}-\boldsymbol{C}_n\right\|_2$	1.65e-01	1.48e-02	6.04e-05	6.48e-09

The analytical $P_i(\lambda)$-relations for UT, ET and PS as required to check the performance of the model on the Treloar data can be derived from Eq. (134), which simplifies considerably since $\partial\Lambda_k/\partial\lambda_i = \delta_{ki}$ due to (136). After inserting the deformation specific principal stretches $\lambda_{1,2,3}$ as given in Subsections 3.1.1...3 and together with Padé approximation (130) of (135) one finally obtains

$$P_1^{UT} = \frac{1}{3}\mu^{UT}\left[\frac{3\lambda N^{UT}-\lambda^3}{N^{UT}-\lambda^2} - \lambda^{-2}\frac{3N^{UT}-\lambda^{-1}}{N^{UT}-\lambda^{-1}}\right] \tag{141}$$

$$P_{1,2}^{ET} = \frac{1}{3}\mu^{ET}\left[\frac{3\lambda N^{ET}-\lambda^3}{N^{ET}-\lambda^2} - \lambda^{-5}\frac{3N^{ET}-\lambda^{-4}}{N^{ET}-\lambda^{-4}}\right] \tag{142}$$

$$P_1^{PS} = \frac{1}{3}\mu^{PS}\left[\frac{3\lambda N^{PS}-\lambda^3}{N^{PS}-\lambda^2} - \lambda^{-3}\frac{3N^{PS}-\lambda^{-2}}{N^{PS}-\lambda^{-2}}\right] . \tag{143}$$

Note that these relations become singular in case of stretches λ approaching the square root of N. Fitting each equation to the corresponding Treloar data yields the following optimal material parameter sets:

$$\mu^{UT} = 0.2681\text{ MPa} \quad , \quad \mu^{ET} = 0.3584\text{ MPa} \quad , \quad \mu^{PS} = 0.3137\text{ MPa} \tag{144}$$

$$N^{UT} = 77.29 \quad , \quad N^{ET} = 45.41 \quad , \quad N^{PS} = 165.3\,. \tag{145}$$

Figure 17 depicts the resulting curves together with the simulations of the complementary deformation modes not used for parameter identification as well as the errors with respect to Treloar's data. All experimental data are perfectly reproduced whereas the general validity of the parameters is hardly convincing. While the optimised shear moduli have reasonable values, i.e. ET is stiffer than PS which is stiffer than UT, this is not the case for the numbers of Kuhn segments N. These are neither identical, as one would expect due to the physical interpretation, nor does their order reflect the assumption of softer material behaviour due to longer chains. Additionally, all stress-stretch relations yield very similar curves, i.e. their structure is not suited to distinguish between different deformation modes, which is a behaviour already observed for the Neo-Hooke or Gent-Thomas model. Even more important is the fact that optimal ET parameters cannot be used to simulate

UT since the necessary stretch range exceeds the corresponding locking stretch $\sqrt{N^{ET}} = \lambda_{locking}^{ET} = 6.74 < 7.69 = \lambda_{max}^{UT}$, which produces an unphysical pole. Constraining the optimisation procedure by fixed values for N that are suited to capture the whole stretch range is not advisable. The resulting increase of fitting errors is not accompanied by a higher validity of parameters due to the likeness between stress relations, also compare the low impact of the second terms in Eqns. (141...143).

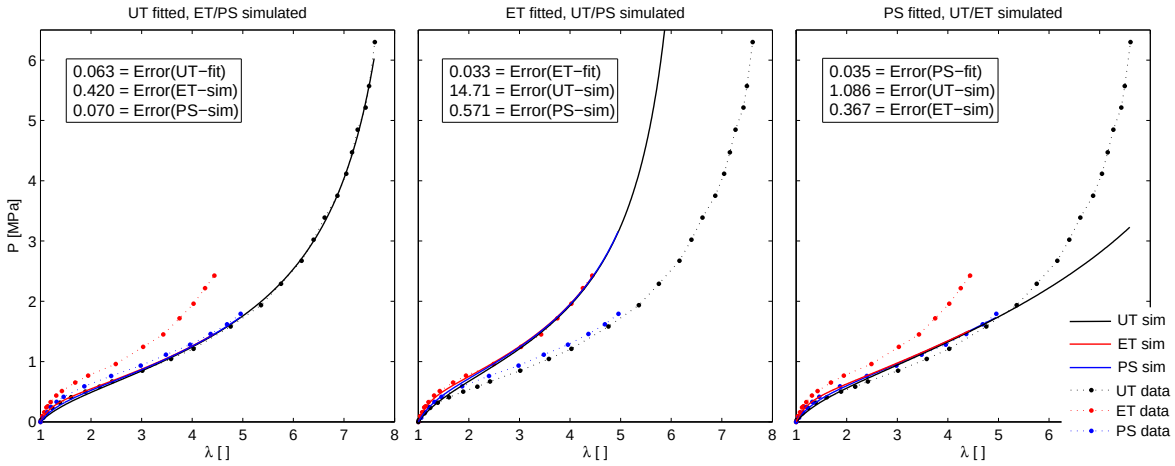

Fig. 17 Performance of the three chain model on the Treloar data. The fitting quality is convincing, especially if compared to models having similarly few parameters like Neo-Hooke or Mooney-Rivlin. Optimised parameters lack a general validity and care must be taken in view of segment numbers and locking stretches.

4.2 Eight chain model (1993)

Similar to the just discussed three chain model, the eight chain approach proposed by Arruda and Boyce [6] is resorting to a cuboid spanned by the principal directions of the isochoric right Cauchy-Green tensor. The local polymer network is – as the name indicates – then approximated by an ensemble of $K = 8$ chains, each of which being oriented along one of the half diagonals of the cuboid, cf. Figure 18. The edge length of the undeformed cube immediately follows as $a_0 = 2\sqrt{3^{-1}}r_0$ from basic geometric considerations, wherein $r_0 = \sqrt{N}l$ is again denoting the end-to-end distance of an unstretched chain. All chains are equally elongated if the surrounding box is deformed with the isochoric principal stretches λ_i. This leads to $r_k = r_0\sqrt{3^{-1}}\sqrt{\lambda_1^2+\lambda_2^2+\lambda_3^2}$ for the new end-to-end distances and one finally obtains

$$\Lambda = \Lambda_k = \frac{r_k}{r_0} = \frac{1}{\sqrt{3}}\sqrt{\lambda_1^2+\lambda_2^2+\lambda_3^2} = \sqrt{\frac{\bar{I}_1}{3}} \quad , \quad k = 1,...,8\,, \tag{146}$$

i.e. a unique stretch which is valid for all chains regardless of their orientation within the cuboid.

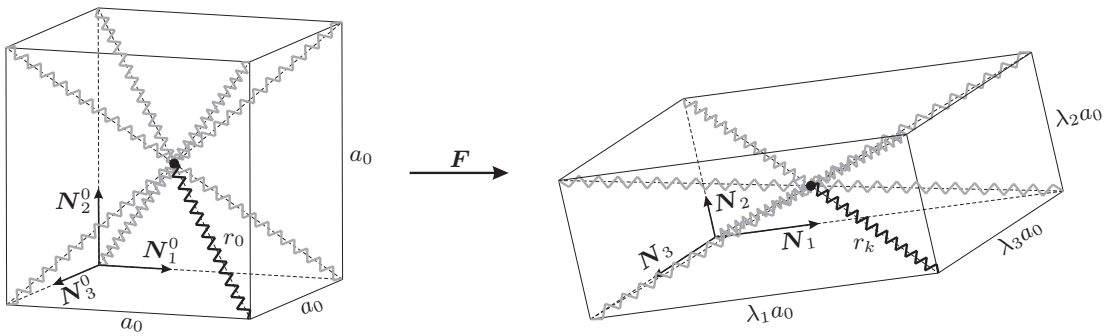

Fig. 18 Eight chain model: initial and deformed chain orientations and stretches

If Langevin chain behaviour is assumed, evaluation of (131) provides

$$\Psi_{\text{iso}} = \frac{n}{8}\sum_{k=1}^{8}\psi^{\text{Langevin}}(\Lambda_k) \overset{(146)}{=} n\psi^{\text{Langevin}}(\Lambda) = \mu N\left[\sqrt{N^{-1}}\Lambda\gamma + \ln\left(\frac{\gamma}{\sinh(\gamma)}\right)\right] \tag{147}$$

for the macroscopic free energy density, wherein $\mu = nk_B\Theta$ is the shear modulus and $\gamma = \mathcal{L}^{-1}(\sqrt{N^{-1}}\Lambda)$ again abbreviates the inverse Langevin function. The corresponding fictitious stress tensor $\bar{\boldsymbol{S}} = 2\partial\Psi_{\text{iso}}/\partial\bar{\boldsymbol{C}}$ is then computed to

$$\bar{\boldsymbol{S}} = \frac{\mu}{3}\left[\frac{3N-\Lambda^2}{N-\Lambda^2}\right]\boldsymbol{I} = \frac{\mu}{3}\left[\frac{9N-\lambda_1^2-\lambda_2^2-\lambda_3^2}{3N-\lambda_1^2-\lambda_2^2-\lambda_3^2}\right]\boldsymbol{I} \tag{148}$$

via the chain rule, applying Padé approximation (130) to Eq. (135) and with $\partial\Lambda/\partial\bar{\boldsymbol{C}} = (6\Lambda)^{-1}\boldsymbol{I}$ since $\partial\bar{I}_1/\partial\bar{\boldsymbol{C}} = \boldsymbol{I}$. According to Eq. (8) the corresponding fictitious tangent operator is then obtained as

$$\bar{\mathbb{C}} = \frac{4}{9}\mu N J^{-\frac{4}{3}}\frac{1}{\left[N-\Lambda^2\right]^2}\boldsymbol{I}\otimes\boldsymbol{I} = \frac{4\mu N J^{-\frac{4}{3}}}{\left[3N-\lambda_1^2-\lambda_2^2-\lambda_3^2\right]^2}\boldsymbol{I}\otimes\boldsymbol{I} \tag{149}$$

from another derivative wrt $\bar{\boldsymbol{C}}$. For material parameters $[\mu, N] = [0.2673\text{ MPa}, 25.84]$, the local convergence test quadratically converges to $\boldsymbol{C}_\infty = [1.66, 2.62, 1.19, 1.66, 0.0, 0.0]$, as is indicated by the following table:

Iteration n	0	1	2	3
$\|\boldsymbol{R}(\boldsymbol{C}_n)\|_2$	5.19e-01	1.19e-01	7.63-04	2.99e-08
$\|\boldsymbol{C}_{n+1}-\boldsymbol{C}_n\|_2$	1.64e-01	1.48e-02	6.11e-05	5.70e-09

The analytical $P_i(\lambda)$-relations for UT, ET and PS are again derived from Eq. (134), which can be simplified beforehand due to identical chain stretches $\Lambda_k = \Lambda$, since $\partial\Lambda/\partial\lambda_i = \lambda_i/3\Lambda$ holds according to (146), and with the usual Padé approximation of Langevin chain force (135):

$$P_i = \frac{\mu}{3}\frac{3N-\Lambda^2}{N-\Lambda^2}\left[\lambda_i - \frac{\lambda_j^2}{\lambda_i}\right] \quad , \quad i\in\{1,2,3\}\ ,\ j \text{ such that } P_j = 0\,. \tag{150}$$

With the deformation dependent squared chain stretches $\Lambda^2_{UT,ET,PS} = \bar{I}_1^{UT,ET,PS}/3$ following from (18), (21) and (24) we finally obtain

$$P_1^{UT} = \frac{\mu^{UT}}{3}\left[\frac{9N^{UT}-\lambda^2-2\lambda^{-1}}{3N^{UT}-\lambda^2-2\lambda^{-1}}\right]\left[\lambda-\lambda^{-2}\right] \tag{151}$$

$$P_{1,2}^{ET} = \frac{\mu^{ET}}{3}\left[\frac{9N^{ET}-2\lambda^2-\lambda^{-4}}{3N^{ET}-2\lambda^2-\lambda^{-4}}\right]\left[\lambda-\lambda^{-5}\right] \tag{152}$$

$$P_1^{PS} = \frac{\mu^{PS}}{3}\left[\frac{9N^{PS}-\lambda^2-\lambda^{-2}-1}{3N^{PS}-\lambda^2-\lambda^{-2}-1}\right]\left[\lambda-\lambda^{-3}\right]\,. \tag{153}$$

Fitting these equations to the corresponding Treloar data provides the following parameter sets:

$$\mu^{UT} = 0.2673\text{ MPa} \quad , \quad \mu^{ET} = 0.3586\text{ MPa} \quad , \quad \mu^{PS} = 0.3124\text{ MPa} \tag{154}$$

$$N^{UT} = 25.84 \quad , \quad N^{ET} = 30.32 \quad , \quad N^{PS} = 55.55\,. \tag{155}$$

Figure 19 depicts the resulting curves as well as simulations of the complementary deformation modes not used for parameter identification. Reproduction of experimental data via fitting is as perfect as for the three chain model while the general validity of parameters is better, although not yet satisfying, and can be compared to that of Yeoh's model. The optimised segment numbers are again neither identical nor do they satisfy the intuitive expectations concerning the stiffnesses of the different deformation modes. It is worth noting that the eight chain model is much less sensitive with respect to locking stretches, i.e. all segment numbers are valid for the whole stretch range.

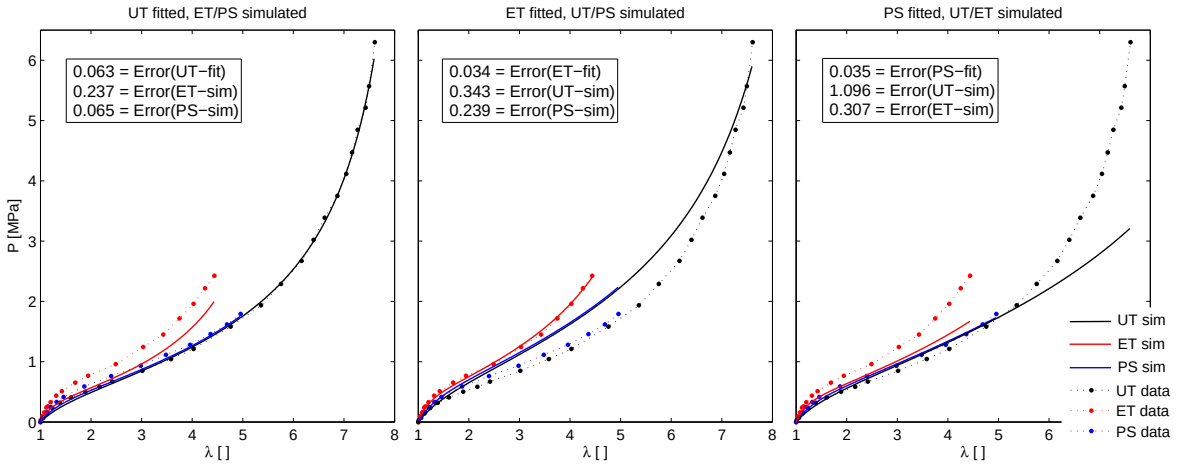

Fig. 19 Performance of the eight chain model on the Treloar data. The fitting quality is convincing but all parameters still lack sufficient generality. Comparable to Yeoh's ansatz the model better distinguishes deformation modes than the three chain version and is not sensitive with respect to locking stretches.

4.3 Twenty-one chain model (2002)

Different to the above discussed three and eight chain models, the twenty-one chain approach proposed by Miehe and co-workers [8], [2], [7], [9] does not consider the $\bar{\boldsymbol{C}}$-eigenvectors cuboid as the confining volume of the local polymer network. It instead resorts to a unit sphere in which the chains are assumed to be oriented along radius vectors from the center to the surface. In the most general case this would require to extend average (131) to an integration over the energies of chains aligned with all possible unit vectors. To avoid a complicated analytical evaluation a numerical scheme inspired by a contribution of Bažant and Oh [58] on the discrete integration over spheres is applied. Similar to a Gauss integration, $K = 21$ unit vectors $\boldsymbol{t}_k^0$ and weight factors w_k are chosen such that an approximately uniform distribution of the chains across the sphere is realised, which ensures isotropic behaviour of the local network. If Langevin chain behaviour is assumed the macroscopic isochoric free energy density follows as

$$\Psi_{\text{iso}} = n \sum_{k=1}^{21} w_k \psi^{\text{Langevin}}(\Lambda_k) = \mu N \sum_{k=1}^{21} w_k \left[\sqrt{N^{-1}} \Lambda_k \gamma_k + \ln \left(\frac{\gamma_k}{\sinh(\gamma_k)} \right) \right], \tag{156}$$

wherein $\mu = n k_B \Theta$ and $\gamma_k = \mathcal{L}^{-1}(\sqrt{N^{-1}} \Lambda_k)$ denote inverse Langevin function of the chain stretches as before. Due to the particular choice of initial chain orientations $\boldsymbol{t}_k^0$, the stretches Λ_k here have to be computed according to Eq. (132)

$$\Lambda_k(\bar{\boldsymbol{C}}) = \sqrt{\boldsymbol{t}_k^0 \cdot \bar{\boldsymbol{C}} \cdot \boldsymbol{t}_k^0}\,, \tag{157}$$

i.e. they do not follow directly in closed form via geometric considerations as has been the case for the three (136) or eight (146) chain models. Coordinates of the $\boldsymbol{t}_k^0$ and the weight factors w_k are summarised in Appendix D for the sake of completeness.
Similar to the derivation for the three chain model, the fictitious stress tensor $\bar{\boldsymbol{S}}$ follows from applying the chain rule to Eq. $(156)_1$, insertion of Padé approximation (130) of Eq. (135) and together with $\partial \Lambda_k / \partial \bar{\boldsymbol{C}} = (2\Lambda_k)^{-1} [\boldsymbol{t}_k^0 \otimes \boldsymbol{t}_k^0]$ as derived in analogy to (138):

$$\bar{\boldsymbol{S}} = 2n \sum_{k=1}^{21} w_k \frac{\partial \psi^{\text{Langevin}}}{\partial \Lambda_k} \frac{\partial \Lambda_k}{\bar{\boldsymbol{C}}} = \mu \sum_{k=1}^{21} w_k \frac{3N - \Lambda_k^2}{N - \Lambda_k^2} [\boldsymbol{t}_k^0 \otimes \boldsymbol{t}_k^0]\,. \tag{158}$$

According to (8) the corresponding fictitious tangent operator then follows from another derivative wrt $\bar{\boldsymbol{C}}$:

$$\bar{\mathbb{C}} = \mu J^{-\frac{4}{3}} \sum_{k=1}^{21} w_k \frac{4N}{[N - \Lambda_k^2]^2} \left[\boldsymbol{t}_k^0 \otimes \boldsymbol{t}_k^0 \otimes \boldsymbol{t}_k^0 \otimes \boldsymbol{t}_k^0 \right]. \tag{159}$$

If the parameters are chosen as $[\mu, N] = [0.3128\ \text{MPa}, 63.74]$ the local tangent test quadratically converges to $\boldsymbol{C}_\infty = [1.67, 2.64, 1.92, 1.68, 0.0, 0.0]$, cf. the evolutions of residuals and strain updates:

Iteration n	0	1	2	3
$\|\boldsymbol{R}(\boldsymbol{C}_n)\|_2$	5.21e-01	1.18e-01	7.56-04	3.27e-08
$\|\boldsymbol{C}_{n+1} - \boldsymbol{C}_n\|_2$	1.65e-01	1.48e-02	6.04e-05	6.48e-09

To derive analytical relations $P_i(\lambda)$ for UT, ET and PS we depart from

$$P_i = n \sum_{k=1}^{21} w_k \frac{\partial \psi^{\text{Langevin}}}{\partial \Lambda_k} \left[\frac{\partial \Lambda_k}{\partial \lambda_i} - \frac{\lambda_j}{\lambda_i} \frac{\partial \Lambda_k}{\partial \lambda_j} \right] \quad , \quad j \ \text{ such that } \ P_j = 0 \,, \tag{160}$$

as obtained by insertion of energy density $(156)_1$ into $(134)_1$. The here included chain forces $\partial \psi^{\text{Langevin}} / \partial \Lambda_k$ are again substituted by Padé approximation (130) of (135) into which the deformation specific chain stretches

$$\Lambda_k^{UT} = \sqrt{\lambda^2 t_{k1} + \frac{t_{k2}}{\lambda} + \frac{t_{k3}}{\lambda}} \,, \; \Lambda_k^{ET} = \sqrt{\lambda^2 t_{k1} + \lambda^2 t_{k2} + \frac{t_{k3}}{\lambda^4}} \,, \; \Lambda_k^{PS} = \sqrt{\lambda^2 t_{k1} + t_{k2} + \frac{t_{k3}}{\lambda^2}} \tag{161}$$

dependent on the applied macrostretch λ have to be inserted. These are easily obtained by evaluation of (157) with the corresponding isochoric right Cauchy-Green strain tensors $\bar{\boldsymbol{C}}$, which in turn have to be computed from the particular deformation gradients given in Eqns. $(18)_1$,$(21)_1$ and $(24)_1$. For the sake of simplicity, we have introduced

$$t_{ki} := [\boldsymbol{e}_i \cdot \boldsymbol{t}_k^0]^2 \tag{162}$$

to abbreviate the squared Cartesian coordinates of the initial chain orientation vectors, cf. Appendix D. The derivatives of the chain stretches wrt the principal stretches appearing in (160) require the consideration of spectral decomposition

$$\bar{\boldsymbol{C}} = \sum_{a=1}^{3} \lambda_a^2 \, \boldsymbol{N}_a \otimes \boldsymbol{N}_a \,. \tag{163}$$

Inserted into (157) we find

$$\begin{aligned} \frac{\partial \Lambda_k}{\partial \lambda_i} &\overset{(157)}{=} \frac{\partial}{\partial \lambda_i} \sqrt{\boldsymbol{t}_k^0 \cdot \bar{\boldsymbol{C}} \cdot \boldsymbol{t}_k^0} = \frac{1}{2\Lambda_k} \frac{\partial}{\partial \lambda_i} \left(\boldsymbol{t}_k^0 \cdot \textstyle\sum_{a=1}^3 \lambda_a^2 \, \boldsymbol{N}_a \otimes \boldsymbol{N}_a \cdot \boldsymbol{t}_k^0 \right) \\ &= \frac{1}{2\Lambda_k} \frac{\partial}{\partial \lambda_i} \left(\textstyle\sum_{a=1}^3 \lambda_a^2 \, \boldsymbol{t}_k^0 \cdot [\boldsymbol{N}_a \otimes \boldsymbol{N}_a] \cdot \boldsymbol{t}_k^0 \right) = \frac{1}{2\Lambda_k} \sum_{a=1}^{3} \frac{\partial}{\partial \lambda_i} \left(\lambda_a^2 \, \left[\boldsymbol{N}_a \cdot \boldsymbol{t}_k^0 \right]^2 \right) , \end{aligned} \tag{164}$$

i.e. the general computation of these derivatives necessitates the eigenvectors $\boldsymbol{N}_a$ of $\bar{\boldsymbol{C}}$. Since the here considered UT, ET and PS provide diagonal deformation gradients, the eigenvectors are not rotated from their reference orientation and we may identify $\boldsymbol{N}_a = \boldsymbol{e}_a$, which allows to further simplify Eq. (164):

$$\frac{\partial \Lambda_k}{\partial \lambda_i} = \frac{1}{2\Lambda_k} \sum_{a=1}^{3} \frac{\partial}{\partial \lambda_i} \left(\lambda_a^2 \, \left[\boldsymbol{e}_a \cdot \boldsymbol{t}_k^0 \right]^2 \right) \overset{(162)}{=} \frac{1}{2\Lambda_k} \sum_{a=1}^{3} 2\lambda_a \, \delta_{ai} \, t_{ka} = \frac{\lambda_i \, t_{ki}}{\Lambda_k} \,. \tag{165}$$

If we now reformulate (160) with (130) of (135) and the squares of chain stretches (161), with (165) and $\lambda_2^{UT}/\lambda_1^{UT} = \lambda^{-3/2}$, $\lambda_3^{ET}/\lambda_1^{ET} = \lambda^{-3}$, $\lambda_3^{PS}/\lambda_1^{PS} = \lambda^{-2}$ (cf. Sections 3.1.1...3), the desired stress-stretch relations finally read:

$$P_1^{UT} = \mu^{UT} \sum_{k=1}^{21} w_k \frac{3N^{UT} - \lambda^2 t_{k1} - \lambda^{-1}[t_{k2} + t_{k3}]}{N^{UT} - \lambda^2 t_{k1} - \lambda^{-1}[t_{k2} + t_{k3}]} \left[\lambda t_{k1} - \frac{t_{k2}}{\lambda^2} \right] \tag{166}$$

$$P_{1,2}^{ET} = \mu^{ET} \sum_{k=1}^{21} w_k \frac{3N^{ET} - \lambda^2 [t_{k1} + t_{k2}] - \lambda^{-4} t_{k3}}{N^{ET} - \lambda^2 [t_{k1} + t_{k2}] - \lambda^{-4} t_{k3}} \left[\lambda t_{k1} - \frac{t_{k3}}{\lambda^5} \right] \tag{167}$$

$$P_1^{PS} = \mu^{PS} \sum_{k=1}^{21} w_k \frac{3N^{PS} - \lambda^2 t_{k1} - t_{k2} - \lambda^{-2} t_{k3}}{N^{PS} - \lambda^2 t_{k1} - t_{k2} - \lambda^{-2} t_{k3}} \left[\lambda t_{k1} - \frac{t_{k3}}{\lambda^2} \right] . \tag{168}$$

These equations are not very handy but can be shortened before implementation by exploiting $\sum t_{ki} = 1$ valid for the initial chain orientations and further by collecting the summands having identical t_{ki} and w_k values into nine groups, cf. Appendix D. Fitting to the corresponding Treloar data then yields

$$\mu^{UT} = 0.3128 \text{ MPa} \quad , \quad \mu^{ET} = 0.3601 \text{ MPa} \quad , \quad \mu^{PS} = 0.3131 \text{ MPa} \tag{169}$$

$$N^{UT} = 63.74 \quad , \quad N^{ET} = 38.02 \quad , \quad N^{PS} = 101.3 \tag{170}$$

for the optimal material parameter sets. Figure 20 shows the fitted curves, the simulations of complementary deformation modes as well as the errors wrt Treloar's data. The reproduction of experimental data by fitting is quite acceptable, although the errors are slightly higher than for some of the phenomenological models. Unconstrained optimisation induces the already discussed inconsistencies concerning the segment number N, fitting ET-data in particular yields a locking stretch $\sqrt{N^{ET}} = 6.17$ far to small for the UT strain range. Furthermore, the structural differences between analytical relations (166)...(168) are not sufficient to discriminate the deformation modes, i.e. material parameters cannot be considered as universally valid. This situation improves significantly if the affinity assumption contained in (132) is substituted by more sophisticated approaches to link chain and macro stretches, like in the eight chain model or the general ansatz proposed in [2]. Further improvement is obtained by so-called tube constraints which additionally account for an increasingly hindered chain stretch due to the lateral contraction of the whole network, also cf. [2] or [9].

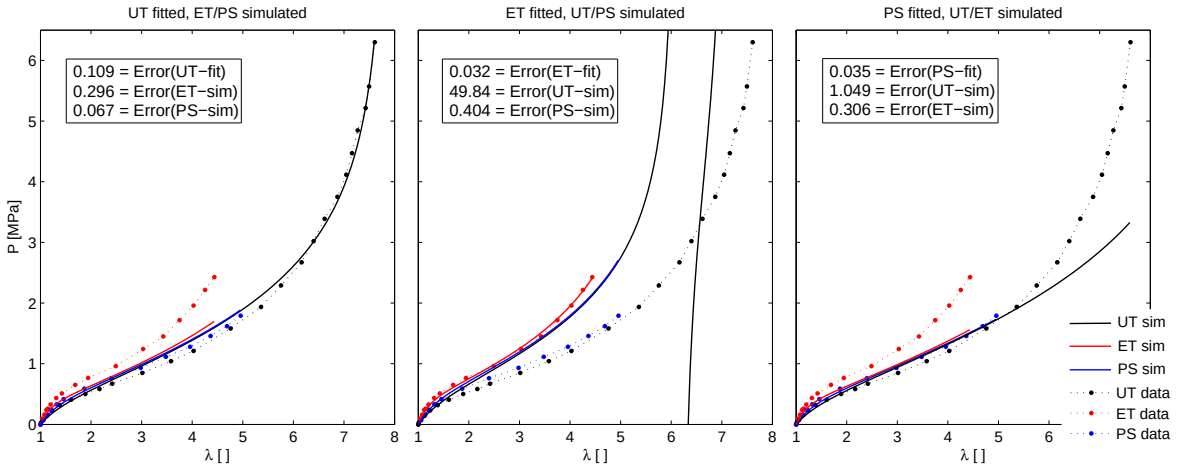

Fig. 20 Performance of the twenty-one chain model on the Treloar data.

5 Conclusions

This contribution presents a survey on fourteen representatives out of the large number of hyperelastic models for rubber-like materials. Special focus is given to the derivation of accurate tangent operators which are indispensable to ensure quadratic convergence when boundary value problems are to be solved by Newton-like iterative schemes. Such derivations traditionally are quite time consuming for a beginner in this field and we hope that the present pages may occasionally be of some assistance. Especially the test procedure of Appendix B together with convergence tables and material parameters given for every model should be suited to check the correctness of own codes for stress tensors and tangent operators.
To evaluate the performance of a particular model is similarly challenging, especially if the experimental data available are limited. In this context it is usually helpful to quickly get an impression on the general behaviour of a model by optimising it with respect to one-dimensional measurements, which in turn can be obtained easily in many cases. The ingredients necessary for such fitting procedures have also been derived for all fourteen models and their application to the classical elastomer data of Treloar can hopefully provide some hints concerning choice or design of a model for a particular application.

Acknowledgements Financial support by the German Research Foundation within PAK 108 is gratefully acknowledged.

References

1. Treloar LRG (1944) Stress-strain data for vulcanised rubber under various types of deformation. Transactions of the Faraday Society 40: 59-70
2. Miehe C, Göktepe S, Lulei F (2004) A micro-macro approach to rubber-like materials - Part I: The non-affine micro-Sphere model of rubber elasticity. Journal of the Mechanics and Physics of Solids 52: 2617-2660
3. Amin AFMS, Lion A, Sekita S, Okui Y (2006) Nonlinear dependence of viscosity in modeling the rate-dependent response of natural and high damping rubbers in compression and shear: Experimental identification and numerical verification. International Journal of Plasticity 22: 1610-1657
4. Boyce MC, Arruda EM (2000) Constitutive models of rubber elasticity: a review. Rubber Chemistry and Technology 73: 504-523
5. Elías-Zúñiga A, Beatty MF(2002)Constitutive equations for amended non-Gaussian network models of rubber elasticity. International Journal of Engineering Science 40: 2265-2294
6. Arruda EM, Boyce MC (1993) A three-dimensional constitutive model for the large stretch behavior of rubber elastic materials. Journal of the Mechanics and Physics of Solids 41: 389-412
7. Miehe C, Göktepe S (2005) A micro-macro approach to rubber-like materials - Part II: The micro-sphere model of finite rubber viscoelasticity. Journal of the Mechanics and Physics of Solids 53: 2231-2258
8. Lulei F (2002) Mikromechanisch motivierte Modelle zur Beschreibung finiter Deformationen gummiartiger Polymere: Physikalische Modellbildung und numerische Simulation. Dissertation. Universität Stuttgart, Germany
9. Göktepe S (2007) Micro-macro approaches to rubbery and glassy polymers: Predictive micromechanically-based models and simulations. Dissertation. Universität Stuttgart, Germany
10. Ogden RW (1972) Large deformation isotropic elasticity - on the correlation of theory and experiment for incompressible rubberlike solids. Proceedings of the Royal Society of London. Series A, Mathematical and Physical Siences 326: 565-584
11. Mooney M (1940) A theory of large elastic deformation. Journal of Applied Physics 11: 582-596
12. Rivlin RS (1948) Large elastic deformations of isotropic materials. IV. Further developments of the general theory. Philosophical Transactions of the Royal Society of London A241: 379-397
13. Rivlin RS (1949) Large elastic deformations of isotropic materials. V. The problem of flexure. Proceedings of the Royal Society of London A195: 463-473
14. Rivlin RS (1949) Large elastic deformations of isotropic materials. VI. Further results in the theory of torsion, shear and flexure. Philosophical Transactions of the Royal Society of London A242: 173-195
15. Yeoh OH (1993) Some forms of the strain energy function for rubber. Rubber Chemistry and Technology 66: 754-771
16. Yeoh OH, Fleming PD (1997) A new attempt to reconcile the statistical and phenomenological theories of rubber elasticity. Journal of Polymer Science Part B: Polymer Physics 35: 1919-1931
17. Wu PD, van der Giessen E (1992) On improved 3-D non-Gaussian network models for rubber elasticity. Mechanics Research Communications 19: 427-433
18. Wu PD, van der Giessen E (1993) On improved network models for rubber elasticity and their applications to orientation hardening in glassy polymers. Journal of the Mechanics and Physics of Solids 41: 427-456
19. Beda T, Chevalier Y (2003) Hybrid continuum model for large elastic deformation of rubber. Journal of Applied Physics 94: 2701-2706
20. Marckmann G, Verron E (2006) Comparison of hyperelastic models for rubber-like materials. Rubber Chemistry and Technology 79: 835-858
21. Kaliske M, Heinrich G (1999) An extended tube-model for rubber elasticity: Statistical mechanical theory and finite element implementation. Rubber Chemistry and Technology 72: 602-632
22. Shariff MHBM (2000) Strain energy function for filled and unfilled rubber-like material. Rubber Chemistry and Technology 73: 1-18
23. Seibert DJ, Schöche N (2000) Direct comparison of some recent rubber elasticity models. Rubber Chemistry and Technology 73: 366-384
24. Attard MM, Hunt GW (2004) Hyperelastic constitutive modeling under finite strain. International Journal of Solids and Structures 41: 5327-5350
25. Valanis KS, Landel RF (1967) The strain-energy function of a hyperelastic material in terms of the extension ratios. Journal of Applied Physics 7: 2997-3002
26. Vangerko H, Treloar LRG (1978) The inflation and extension of rubber tube for biaxial strain studies. Journal of Physics D: Applied Physics 11: 1969-1978
27. Chagnon G, Marckmann G, Verron E (2004) A comparison of the Hart-Smith model with Arruda-Boyce and Gent formulations for rubber elasticity. Rubber Chemistry and Technology 77: 724-735
28. Hart-Smith LJ (1966) Elasticity parameters for finite deformations of rubber like materials. Zeitschrift für Angewandte Mathematik und Physik 17: 608-626
29. Gent AN (1996) A new constitutive relation for rubber. Rubber Chemistry and Technology 69: 59-61
30. Boyce MC (1996) Direct comparison of the Gent and Arruda-Boyce constitutive models of rubber elasticity. Rubber Chemistry and Technology 69: 781-785
31. Horgan CO, Saccomandi G (1999) Simple torsion of isotropic, hyperelastic, incompressible materials with limiting chain extensibility. Journal of Elasticity 56: 159-170
32. Horgan CO, Saccomandi G (2002) A molecular-statistical basis for the Gent constitutive model of rubber elasticity. Journal of Elasticity 68: 167-176
33. Currie PK (2005) Comparison of incompressible elastic strain energy functions over the attainable region of invariant space. Mathematics and Mechanics of Solids 10: 559-574
34. Haines DW, Wilson WD (1979) Strain-energy density function for rubberlike materials. Journal of the Mechanics and Physics of Solids 27: 345-360

35. Miehe C (1994) Aspects of the formulation and finite element implementation of large strain isotropic elasticity. International Journal for Numerical Methods in Engineering 37: 1981-2004
36. Liu CH, Hofstetter G, Mang HA (1994) 3D finite element analysis of rubber-like materials at finite strains. Engineering Computations 11: 111-128
37. Kaliske M, Rothert H (1997) On the finite element implementation of rubber-like materials at finite strains. Engineering Computations 14: 216-232
38. Heinrich G, Kaliske M (1997) Theoretical and numerical formulation of molecular based constitutive tube-model of rubber elasticity. Computational and Theoretical Polymer Science 7: 227-241
39. Isihara A, Hashitsume N, Tatibana M (1951) Statistical theory of rubber-like elasticity. IV. (Two-dimensional stretching). Journal of Chemical Physics 19: 1508-1512
40. Gent AN, Thomas AG (1958) Forms for the stored (strain) energy function for vulcanized rubber. Journal of Polymer Science 28: 625-628
41. Thomas AG (1955) The departures from the statistical theory of rubber elasticity. Transactions of the Faraday Society 51: 569-582
42. Holzapfel GA (2001) Nonlinear solid mechanics. John Wiley & Sons, Chichester
43. Swanson SR (1985) A constitutive model for high elongation elastic materials. Journal of engineering materials and technology 107: 110-115
44. Swanson SR, Christensen LW, Ensign M (1985) Large deformation finite element calculations for slightly compressible hyperelastic materials. Computers & Structures 21: 81-88
45. Yeoh OH (1990) Characterization of elastic properties of carbon-black-filled rubber vulcanizates. Rubber Chemistry and Technology 63: 792-805
46. Biderman VL (1958) Calculation of rubber parts (russian). Rascheti na Prochnost 40
47. James HM, Guth E (1943) Theory of the elastic properties of rubber. Journal of Chemical Physics 11: 455-481
48. Wang MC, Guth E (1952) Statistical theory of networks of non-Gaussian flexible chains. Journal of Chemical Physics 20: 1144-1157
49. Bergström JS, Boyce MC (1998) Constitutive modeling of the large strain time-dependent behavior of elastomers. Journal of the Mechanics and Physics of Solids 46: 931-954
50. Flory PJ (1961) Thermodynamic relations for high elastic materials. Transactions of the Faraday Society 57: 829-838
51. Reese S, Govindjee S (1998) A theory of finite viscoelasticity and numerical aspects. International Journal of Solids and Structures 35: 3455-3482
52. Başar Y, Weichert D (2000) Nonlinear continuum mechanics of solids. Fundamental mathematical and physical concepts. Springer, Berlin
53. Bonet J, Wood RD (1997) Nonlinear continuum mechanics for finite element analysis. Cambridge University Press, Cambridge
54. Treloar LRG (1975) The physics of rubber elasticity. Clarendon Press, Oxford
55. Wriggers P (2001) Nichtlineare Finite-Element Methoden, Springer, Berlin
56. Böl M (2005) Numerische Simulation von Polymernetzwerken mit Hilfe der Finite-Elemente-Methode. PhD thesis, Ruhr-University Bochum, Germany
57. Kuhn W (1942) Über die Gestalt fadenförmiger Moleküle in Lösungen. Kolloid-Zeitschrift 68: 2-15
58. Bažant ZP, Oh BH (1986) Efficient numerical integration on the surface of a sphere. Zeitschrift für Angewandte Mathematik und Mechanik 66: 37-49
59. Nah C, Lee GB, Lim JY, SenGupta R, Gent AN (2010) Problems in determining the elastic strain energy function for rubber. International Journal of Non-Linear Mechanics 45: 232-235
60. Miehe C (1993) Computation of isotropic tensor functions. Communications in Numerical Methods in Engineering 9: 889-896
61. Simo JC, Taylor RL (1991) Quasi-incompressible finite elasticity in principal stretches. Continuum basis and numerical algorithms. Computer Methods in Applied Mechanics and Engineering 85: 273-310
62. Carroll MM (2011) A strain energy function for vulcanized rubbers. Journal of Elasticity 103: 173-187

Appendix A: Treloar Data

To evaluate the performance of particular constitutive models for elastomers it is common practice to test their ability to reproduce the classic experimental data of Treloar [1]. Most publications only mention that these data have been used, some others like Arruda and Boyce [6] at least plot the data used, but numbers cannot be found in the literature so far. To remedy this deficiency, we give the quantitative details as derived from the original paper of Treloar [1], who extensively investigated the behaviour of vulcanised rubber containing 8% of sulphur. A standard graphics software has been used to extract pairs of stretch values and corresponding Piola stresses from the curves for uniaxial tension (UT, p. 63), pure shear (PS, p. 66) and equibiaxial tension (ET, p. 62) given in [1]. For the latter case, the originally plotted stress values additionally had to be multiplied by the stretch to obtain the Piola stress. Different to various other authors we use the complete set of experimental data for fitting, i.e. deviations in the material parameters obtained here and elsewhere are explicable by differences in the chosen (sub)sets of experimental data as well as in numeric deviations caused by the data extraction.

Experimental data for UT, PS and ET of vulcanised rubber containing 8% sulphur, as extracted from Treloar [1]:

uniaxial tension		pure shear		equibiaxial tension	
λ [ ]	P [MPa]	λ [ ]	P [MPa]	λ [ ]	P [MPa]
1.00	0.00	1.00	0.00	1.00	0.00
1.01	0.03	1.06	0.07	1.04	0.09
1.12	0.14	1.14	0.16	1.08	0.16
1.24	0.23	1.21	0.24	1.12	0.24
1.39	0.32	1.32	0.33	1.14	0.26
1.61	0.41	1.46	0.42	1.20	0.33
1.89	0.50	1.87	0.59	1.31	0.44
2.17	0.58	2.40	0.76	1.42	0.51
2.42	0.67	2.98	0.93	1.69	0.65
3.01	0.85	3.48	1.11	1.94	0.77
3.58	1.04	3.96	1.28	2.49	0.96
4.03	1.21	4.36	1.46	3.03	1.24
4.76	1.58	4.69	1.62	3.43	1.45
5.36	1.94	4.96	1.79	3.75	1.72
5.76	2.29			4.03	1.96
6.16	2.67			4.26	2.22
6.40	3.02			4.44	2.43
6.62	3.39				
6.87	3.75				
7.05	4.12				
7.16	4.47				
7.27	4.85				
7.43	5.21				
7.50	5.57				
7.61	6.30				

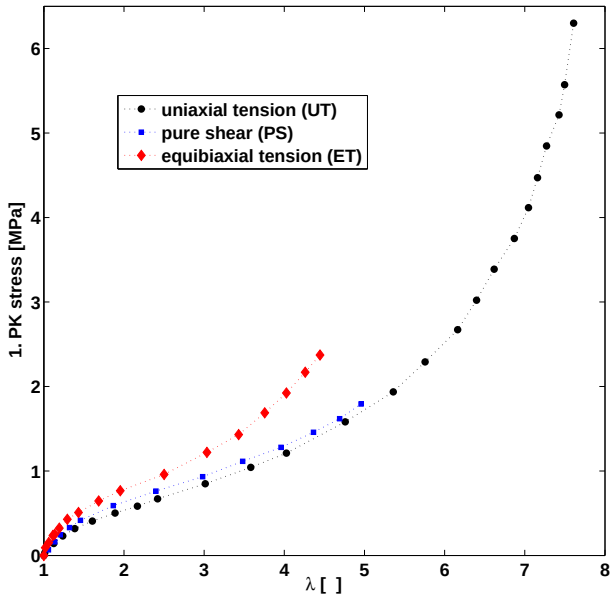

It is important to note that these deformations are by far not reversible, but, in fact, are revealing significant inelastic characteristics if stretches $\lambda \geq 3...4$ are applied, cf. the original plots in [1] or [54]. This behaviour, which is frequently explained by strain-induced crystallisation, had been paid particular attention already by Treloar himself. Recently, Gent et al. [59] have pointed out again that it is, therefore, not appropriate to use strain energy functions to model rubber-like materials, at least not for the very large strain data on lightly cross-linked natural rubber as published by Treloar. It was further concluded from a universal relation between torsional stiffness and tensile stress derived by Rivlin [14], that it is at least doubtful to apply hyperelasticity to 'a typical elastic solid' strained more than 300%. As a method to determine the range of deformation that is valid for a material to be described by a strain energy function the so-called Mooney-Rivlin plot comparing torsional and tensile behaviour is recommended.

Despite the limited reversibility of Treloar's stress-strain data, the whole strain range is employed here to identify the material parameters and to evaluate the models for the following reason. Various other elastomers are known to deform reversibly while simultaneously exhibiting certain characteristics observable in Treloar's data, e.g. large strains and the typical S-shape. We therefore consider these data as a prototype or worst-case scenario of highly non-linear behaviour, which one might want to reproduce by using hyperelastic models, and tacitly ignore that they originate from an inelastic material. Thus, all parameters given in the previous sections have to be understood as valid for a fictitious, highly non-linear elastic material rather than for slightly cross-linked natural rubber as used by Treloar. To assess the performance of the models with respect to this particular material, all fitting procedures have to be repeated on the subset of reversible deformations, which is postponed to a later contribution since it would inadmissibly extend the scope of this work.

Appendix B: A local check for quadratic convergence

A desirable feature of numerical solutions of continuum mechanical boundary value problems by iterative techniques is to obtain a quadratic convergence rate. This property is given if the tangent operator used to update the stress state in consequence of a new strain increment is thermodynamically consistent. To prove quadratic convergence for the tangent operators given in this contribution, i.e. to assure properness of derivation and implementation, we use a simple but effective local method described in the following.
Both the 2^{nd} Piola-Kirchhoff stress $\boldsymbol{S}$ as well as the material tangent operator $\mathbb{C}$ are given by the free energy Ψ according to Eqs. (1), i.e. they depend on the right Cauchy-Green tensor $\boldsymbol{C}$. By prescribing a particular stress state $\boldsymbol{S}_\infty = \textbf{const.}$, we can formulate the computation of the corresponding strain state $\boldsymbol{C}_\infty$ of a particular constitutive model as to calculate the root of the nonlinear tensor-valued residual

$$\boldsymbol{R}(\boldsymbol{C}) := \boldsymbol{S}_\infty - 2\frac{\partial \Psi(\boldsymbol{C})}{\partial \boldsymbol{C}} = \boldsymbol{S}_\infty - \boldsymbol{S}(\boldsymbol{C}) \stackrel{!}{=} 0. \tag{171}$$

This can be solved using Newton's method, i.e. by incrementally updating the strain tensor according to $\boldsymbol{R}'(\boldsymbol{C}_n) : \Delta\boldsymbol{C} = -\boldsymbol{R}(\boldsymbol{C}_n)$. The required 4^{th}-order Jacobian $\boldsymbol{R}'$ coincides with the tangent operator:

$$\boldsymbol{R}'(\boldsymbol{C}_n) = \left.\frac{\partial \boldsymbol{R}(\boldsymbol{C})}{\partial \boldsymbol{C}}\right|_{\boldsymbol{C}_n} = -\frac{1}{2}4\left.\frac{\partial^2 \Psi(\boldsymbol{C})}{\partial \boldsymbol{C}^2}\right|_{\boldsymbol{C}_n} = -\frac{1}{2}\mathbb{C}(\boldsymbol{C}_n), \tag{172}$$

i.e. one has to solve

$$\frac{1}{2}\mathbb{C}(\boldsymbol{C}_n) : [\boldsymbol{C}_{n+1} - \boldsymbol{C}_n] = \boldsymbol{S}_\infty - \boldsymbol{S}(\boldsymbol{C}_n). \tag{173}$$

By exploiting symmetry and using Voigt's notation this reduces to a matrix-vector equation, i.e. to the solution of a six-dimensional system of equations. If the initial strain $\boldsymbol{C}_0$ is chosen close enough to the solution the method will yield quadratic convergence, i.e. it provides a simple but general method to check accuracy and consistency of arbitrary tangent operators – without a complete finite element implementation.
The introduced method is realised by the following Matlab code which calls the two functions `Stress` and `Tangent` containing the calculation of $\boldsymbol{S}(\boldsymbol{C}_n)$ and $\mathbb{C}(\boldsymbol{C}_n)$ according to the analytical formulations derived in the particular subsection of each model. For the prescribed stress state we have chosen a value of $\boldsymbol{S}_\infty = [6.55, 4.3, 3.5, -3.9, 0.0, 0.0]$ while for the initial strain state $\boldsymbol{C}_0 = [1.55, 2.5, 1.2, 1.5, 0.1, 0.1]$ is used. Both evolutions of the Euclidean norm of the strain updates $\|\boldsymbol{C}_{n+1} - \boldsymbol{C}_n\|_2$ and the residuals $\|\boldsymbol{R}(\boldsymbol{C}_n)\|_2$ are given. Quadratic convergence, i.e. consistency of derivation, is indicated if the number of correct digits is doubled in every iteration. Furthermore, the final strain state $\boldsymbol{C}_\infty = [C_{xx}, C_{yy}, C_{zz}, C_{xy}, C_{xz}, C_{yz}]$ corresponding to $\boldsymbol{S}_\infty$ is given. This value will naturally be unique for each model since it is defined by the initial value $\boldsymbol{C}_0$ (being the same for all models) and the choice of the material parameters.

```
function [nit] = convergence_check(C_0,S_infty,Iterations)
C_n = C_0;
Jac = zeros(6,6);
Tol = 1.0e-8;
for i = 1:Iterations
    C_old = C_n;
    R = Stress(C_n)-S_infty;
    Jac = Tangent(C_n);
    Jac(1:6,4:6) = 2*Jac(1:6,4:6);
    Delta = Jac\(-R');
    C_n = C_n + Delta;
    Diff = norm(C_n-C_old,2);
    if Diff <= Tol
        break;
    end
    if i == Iterations
        fprintf('Solution cannot converge with number of Iterations');
        break;
    end
    nit = i;
end
```

Appendix C: $\dfrac{\partial\left(\boldsymbol{N}_k^0 \otimes \boldsymbol{N}_k^0\right)}{\partial \bar{\boldsymbol{C}}}$

The computation of the derivatives of the eigenvector dyads with respect to $\bar{\boldsymbol{C}}$ as required in the tangent operator $\mathbb{C}$ of the three chain model is summarised here for the sake of completeness. For a proof and more details see e.g. [60]. With definitions

$$\boldsymbol{M}_k = \boldsymbol{N}_k^0 \otimes \boldsymbol{N}_k^0 \tag{174}$$

$$D_k = 2\lambda_k^4 - \lambda_k^2 \bar{I}_1 + \frac{\bar{I}_3}{\lambda_k^2} \tag{175}$$

$$D_k' = \frac{\partial D_k}{\partial \lambda_k^2} = 4\lambda_k^2 - \bar{I}_1 - \frac{\bar{I}_3}{\lambda_k^4} \tag{176}$$

$$\mathbb{I}_{sym} = \frac{1}{2}\left[\delta_{ik}\delta_{jl} + \delta_{il}\delta_{jk}\right] \tag{177}$$

$$\mathbb{I}_{\bar{\boldsymbol{C}}^{-1}} = \frac{1}{2}\left[\bar{C}_{ik}^{-1}\bar{C}_{jl}^{-1} + \bar{C}_{il}^{-1}\bar{C}_{jk}^{-1}\right] \tag{178}$$

the derivatives read

$$\frac{\partial\left(\boldsymbol{N}_k^0 \otimes \boldsymbol{N}_k^0\right)}{\partial \bar{\boldsymbol{C}}} = \frac{\lambda_k^2}{D_k}\Big[\mathbb{I}_{sym} - \boldsymbol{I}\otimes\boldsymbol{I} - \frac{\bar{I}_3}{\lambda_k^2}\left[\mathbb{I}_{\bar{\boldsymbol{C}}^{-1}} - \bar{\boldsymbol{C}}^{-1}\otimes\bar{\boldsymbol{C}}^{-1}\right] + \boldsymbol{I}\otimes\boldsymbol{M}_k + \boldsymbol{M}_k\otimes\boldsymbol{I} \tag{179}$$

$$- \frac{\bar{I}_3}{\lambda_k^4}\left[\bar{\boldsymbol{C}}^{-1}\otimes\boldsymbol{M}_k + \boldsymbol{M}_k\otimes\bar{\boldsymbol{C}}^{-1}\right] + \frac{D_k - \lambda_k^2 D_k'}{\lambda_k^4}\boldsymbol{M}_k\otimes\boldsymbol{M}_k\Big] \tag{180}$$

Appendix D: Initial chain orientation vectors and weights of the twenty-one chain model

The coefficients w_k and the direction vectors $\boldsymbol{t}_k^0$ required for the twenty-one chain model go back to the work of Bažant and Oh [58]. Both the Cartesian coordinates as well as their squares $t_{ki} = [\boldsymbol{e}_i \cdot \boldsymbol{t}_k^0]^2$ required for the analytical stress-stretch relations (166),(167),(168) are given in the table below for completeness. Subsequent and equally colored lines identify groups of identical values which may be collected into one single summand each by using correspondingly multiplied weights w_k. Note that only a half-sphere is covered by the vectors below, a complete set would require another twenty-one vectors oriented in the opposite directions. These can be substituted by doubling the weights to reduce compuational costs.

k	w_k	$(\boldsymbol{t}_k^0)_1$	$(\boldsymbol{t}_k^0)_2$	$(\boldsymbol{t}_k^0)_3$	t_{k1}	t_{k2}	t_{k3}
1	0.0530428488186	1.000000000000	0.000000000000	0.000000000000	1.000000000000	0.000000000000	0.000000000000
2	0.0530428488186	0.000000000000	1.000000000000	0.000000000000	0.000000000000	1.000000000000	0.000000000000
3	0.0530428488186	0.000000000000	0.000000000000	1.000000000000	0.000000000000	0.000000000000	1.000000000000
4	0.0398602952624	0.707106781187	0.707106781187	0.000000000000	0.500000000000	0.500000000000	0.000000000000
5	0.0398602952624	0.707106781187	-0.707106781187	0.000000000000	0.500000000000	0.500000000000	0.000000000000
6	0.0398602952624	0.707106781187	0.000000000000	0.707106781187	0.500000000000	0.000000000000	0.500000000000
7	0.0398602952624	0.707106781187	0.000000000000	-0.707106781187	0.500000000000	0.000000000000	0.500000000000
8	0.0398602952624	0.000000000000	0.707106781187	0.707106781187	0.000000000000	0.500000000000	0.500000000000
9	0.0398602952624	0.000000000000	0.707106781187	-0.707106781187	0.000000000000	0.500000000000	0.500000000000
10	0.0501424734974	0.387907304067	0.387907304067	0.836095596749	0.150472076549	0.150472076549	0.699055846903
11	0.0501424734974	0.387907304067	0.387907304067	-0.836095596749	0.150472076549	0.150472076549	0.699055846903
12	0.0501424734974	0.387907304067	-0.387907304067	0.836095596749	0.150472076549	0.150472076549	0.699055846903
13	0.0501424734974	0.387907304067	-0.387907304067	-0.836095596749	0.150472076549	0.150472076549	0.699055846903
14	0.0501424734974	0.387907304067	0.836095596749	0.387907304067	0.150472076549	0.699055846903	0.150472076549
15	0.0501424734974	0.387907304067	0.836095596749	-0.387907304067	0.150472076549	0.699055846903	0.150472076549
16	0.0501424734974	0.387907304067	-0.836095596749	0.387907304067	0.150472076549	0.699055846903	0.150472076549
17	0.0501424734974	0.387907304067	-0.836095596749	-0.387907304067	0.150472076549	0.699055846903	0.150472076549
18	0.0501424734974	0.836095596749	0.387907304067	0.387907304067	0.699055846903	0.150472076549	0.150472076549
19	0.0501424734974	0.836095596749	0.387907304067	-0.387907304067	0.699055846903	0.150472076549	0.150472076549
20	0.0501424734974	0.836095596749	-0.387907304067	0.387907304067	0.699055846903	0.150472076549	0.150472076549
21	0.0501424734974	0.836095596749	-0.387907304067	-0.387907304067	0.699055846903	0.150472076549	0.150472076549